# MAGNETICALLY STEERED CELL THERAPY FOR REDUCTION OF INTRAOCULAR PRESSURE AS A TREATMENT STRATEGY FOR OPEN-ANGLE GLAUCOMA

M. Reza Bahrani Fard[1], Jessica Chan[2], A. Thomas Read[3], Guorong Li[4], Lin Cheng[5,6], Babak N. Safa[3,7], Seyed Mohammad Siadat[3], Anamik Jhunjhunwala[3], Hans E. Grossniklaus[8], Stanislav Y. Emelianov[3,9], W. Daniel Stamer[4,10], Markus H. Kuehn[5,6], C. Ross Ethier[1,3]

1. Woodruff School of Mechanical Engineering, Georgia Institute of Technology, Atlanta, Georgia
2. School of Chemistry and Biochemistry, Georgia Institute of Technology, Atlanta, Georgia
3. Wallace H. Coulter Department of Biomedical Engineering, Georgia Institute of Technology/Emory University, Atlanta, Georgia
4. Department of Ophthalmology, Duke University, Durham, NC
5. Departments of Ophthalmology and Visual Sciences, The University of Iowa, Iowa City, IA
6. Veterans Administration Center for the Prevention and Treatment of Visual Loss, Iowa City VA Healthcare System, Iowa City, IA
7. Department of Medical Engineering, University of South Florida, Tampa, FL
8. Departments of Ophthalmology and Pathology, Emory University School of Medicine, Atlanta, GA
9. School of Electrical and Computer Engineering, Georgia Institute of Technology, Atlanta, Georgia
10. Departments of Biomedical Engineering, Duke University, Durham, NC

Corresponding author:

C. Ross Ethier, Ph.D.
Professor and Georgia Research Alliance Eminent Scholar in Bioengineering
Wallace H. Coulter Department of Biomedical Engineering
Georgia Institute of Technology/Emory University
ross.ethier@bme.gatech.edu

## 1. Abstract

Trabecular meshwork (TM) cell therapy has been proposed as a next-generation treatment for elevated intraocular pressure (IOP) in glaucoma, the most common cause of irreversible blindness. Using a magnetic cell steering technique with excellent efficiency and tissue-specific targeting, we delivered two types of cells into a mouse model of glaucoma: either human adipose-derived mesenchymal stem cells (hAMSCs) or induced pluripotent cell derivatives (iPSC-TM cells). We observed a 4.5 [3.1, 6.0] $\mathrm{mmHg}$ or 27% reduction in intraocular pressure (IOP) for nine months after a single dose of only 1500 magnetically-steered hAMSCs, explained by increased outflow through the conventional pathway and associated with an higher TM cellularity. iPSC-TM cells were also effective, but less so, showing only a 1.9 [0.4, 3.3] $\mathrm{mmHg}$ or 13% IOP reduction and increased risk of tumorigenicity. In both cases, injected cells remained detectable in the iridocorneal angle three weeks post-transplantation. Based on the locations of the delivered cells, the mechanism of IOP lowering is most likely paracrine signaling. We conclude that magnetically-steered hAMSC cell therapy has potential for long-term treatment of ocular hypertension in glaucoma.

**One Sentence Summary:** A novel magnetic cell therapy provided effective intraocular pressure reduction in a mouse model, motivating future translational studies.

## 2. Introduction

Glaucoma, an optic neuropathy, is the leading cause of irreversible blindness, with more than 80 million cases worldwide *(1)*. Primary open-angle glaucoma (POAG), the most common subtype of the disease, is characterized by a gradual loss of retinal ganglion cells and a corresponding loss of vision. While the exact mechanism underlying retinal ganglion loss is not well understood, elevated intraocular pressure (IOP) is a major risk factor *(2)*; consequently, all current clinical treatments seek to sustainably lower IOP, using pharmacological, laser, and surgical means. However, the success of such IOP-lowering treatments is reduced by low patient adherence to medical therapies *(3)*, by post-surgical complications, and/or by patients becoming refractory to originally successful treatments *(4)*. Thus, there remains a major unmet public health need for methods that offer sustained IOP control in glaucoma patients.

The trabecular meshwork (TM; Figure 1A) is an ocular tissue that drains the majority of aqueous humor (AH) from the human eye, and its function is a major determinant of IOP. There are a number of age- and glaucoma-associated changes in the TM, including an age-associated loss

of TM cells which is accelerated in POAG *(5)*. This cell deficiency has been identified as a therapeutic target for IOP control in glaucoma patients, with multiple groups attempting to re-functionalize the TM by injection of stem cells into the eye to restore normal IOP homeostasis *(6–14)*.

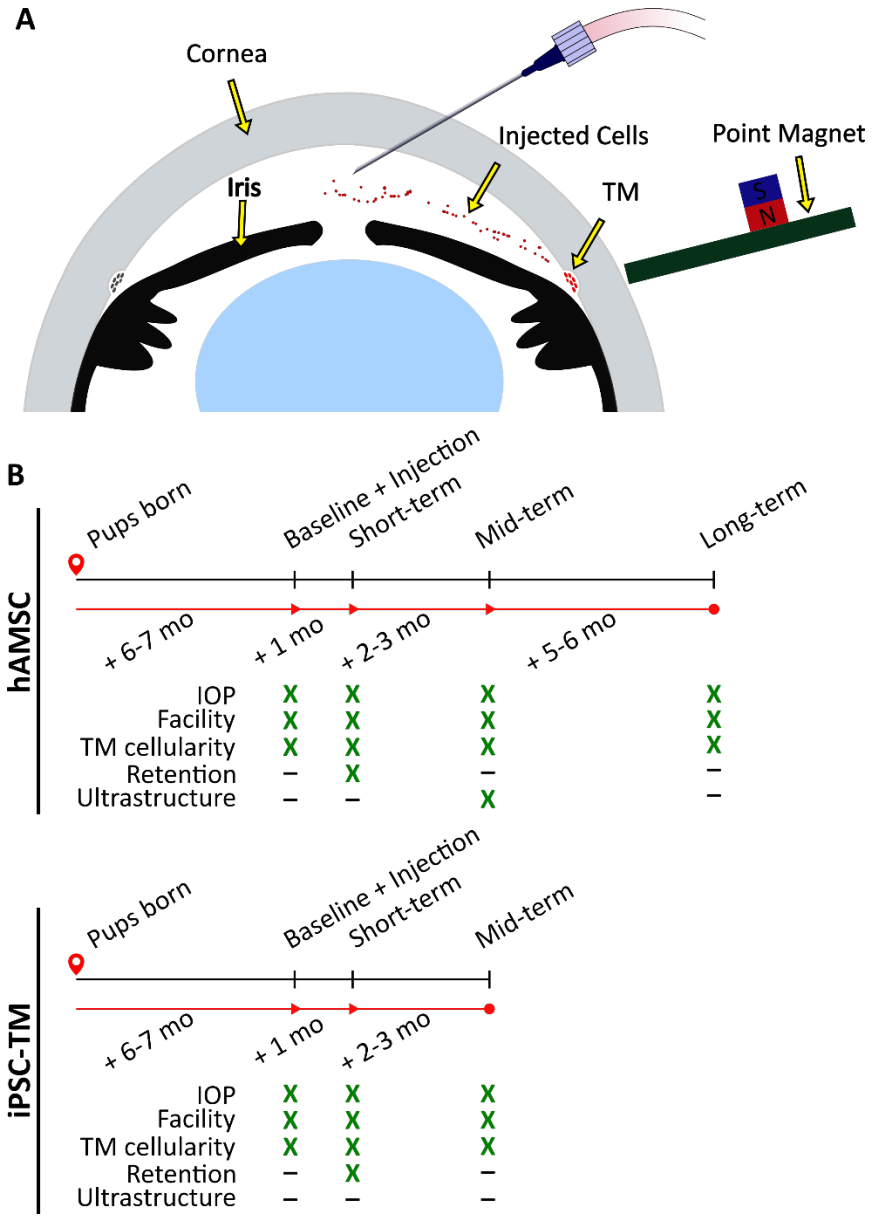


Figure 1. Experimental schematic and design. A) Schematic of magnetically-steered cell delivery to the TM. As cells are injected into the anterior chamber at a low flow rate, the experimenter places the "point magnet" (15) on the limbus and carefully drags the cells towards the iridocorneal angle, targeting the trabecular meshwork (TM). Features of the figure are not drawn to scale. B) Time-line of the experiments. An ultrastructural analysis, specifically the quantification of inner wall basement membrane fenestrations, was not undertaken for eyes receiving iPSC-TMs due to their inferior performance. Additionally, cell retention in the anterior chamber was only

investigated at the short-term. Note that baseline measurements were taken for WT and transgenic animals that did not necessarily receive an injection afterwards. Refer to Methods for a description of various experimental groups and further details.

Despite the potential of stem cell treatment for IOP control, there remain several critical barriers to translation. For example, cell delivery to the TM has typically relied on passive transport of cells by AH outflow, leading to extremely low delivery efficiencies *(16)*. A more efficient delivery method is desirable, which is expected to both increase the therapeutic benefit of the treatment and reduce immunogenicity; for example, Zhou et al. reported an increase in the inflammatory markers CD45 and GR1 and T-cell markers CD4 and CD3 in the iris and the cornea after mesenchymal stem cell injection, likely due to off-target cell delivery *(13)*. We have recently introduced a magnetically-steered cell delivery technique which significantly outperforms previously-used magnetic and non-magnetic delivery techniques *(15)*. Here we characterize the efficacy of our stem cell delivery using this technique to lower IOP.

A second barrier to translation is lack of knowledge about which cell type should be delivered to restore TM function. Three types of cells have previously been used in this context: native TM stem cells (TMSC), mesenchymal stem cells, and induced pluripotent stem cell (iPSC) derivatives. TMSC therapy lowers IOP and increases TM cellularity *(11, 14)*, and is theoretically attractive. However, the scarcity of TMSCs, constituting only 2-5% of the entire TM cell population *(17)*, and the invasiveness of the required cell collection procedure significantly reduce the translational potential of this cell source. Alternatively, mesenchymal stem cells have been used in several studies, showing a transient IOP reduction as well as neuroprotection *(6, 7)*. For example, Manuguerra-Gagné et al. injected bone-marrow derived mesenchymal stem cells in a rat model of IOP elevation, observing a reduction in IOP for three weeks *(6)*. These results, together with the ease of sourcing autologous cells, and the established safety of mesenchymal stem cell therapy in clinical trials *(18, 19)*, make these stem cells a strong candidate for clinical POAG cell therapy. Finally, iPSCs can be differentiated into iPSC-TM cells, with the differentiated cells displaying phenotypic similarity to adult TM cells *(20)*. Intracameral injection of iPSC-TMs into a perfused porcine anterior segment POAG model restored the IOP homeostatic response *(8)*. Additionally, Zhu and colleagues delivered iPSC-TMs into the anterior chambers of ocular hypertensive mice and reported increased TM cellularity due to proliferation of endogenous cells and a corresponding decrease in the IOP for up to 12 weeks after cell delivery *(9, 10)*. Although both MSC and IPSC-TM showed promise, there is no information about their efficacy and safety

104 in comparison to each other. Therefore, here we compare the benefits of mesenchymal stem cells
105 vs. iPSC-TM cells.

106 An additional barrier to translation is the choice of an appropriate animal model for preclinical
107 testing, since no animal model replicates all the pathological phenotypes of POAG. For example,
108 although non-human primate models show high anatomical and functional resemblance to
109 humans and are the gold standard for certain pre-clinical studies *(21)*, induction of ocular
110 hypertension requires laser photocoagulation of the TM, which is very unlike TM changes seen in
111 POAG *(6, 22)*. Microbead *(23)* and hypertonic saline *(24)* models of ocular hypertension are
112 similarly distinct from human POAG pathology. Commercially available DBA/2 mice show TM cell
113 loss and IOP elevation but are associated with undesirable systemic and ocular complications
114 *(25)*. Thus, in this work we chose to use transgenic MYOC$^{Y437H}$ mice. These mice carry a
115 glaucoma-causing point mutation in the MYOC gene, and have been reported to show an
116 accelerated loss of TM cellularity and a gradual ocular hypertension development *(26)*.

117 In summary, we here evaluate the effectiveness of TM cell therapy, using a magnetic cell steering
118 method and two clinically relevant cell choices, namely human adipose-derived mesenchymal
119 stem cells (hAMSCs) and iPSC-TM cells, in MYOC$^{Y437H}$ mice. We judged effectiveness by the
120 extent and longevity of IOP reduction, improvement in outflow facility, and increase in TM
121 cellularity, among other outcome measures, and performed experiments using animal cohorts at
122 different time points (Figure 1 B, detailed in Methods section). Despite the absence of ocular
123 hypertension in our MYOC$^{Y437H}$ mice, our data demonstrate sustained IOP lowering and a
124 significant benefit of magnetic cell steering in the eye, particularly for hAMSCs, strongly indicating
125 further translational potential.

126 **3. Results**

127 *a. Cell transplantation lowered IOP and improved aqueous humor dynamics*

128 We delivered and magnetically steered either hAMSCs or iPSC-TMs to the TM of eyes of
129 MYOC$^{Y437H}$ mice (Figure 1 A), measuring IOPs and outflow facilities at short-, mid-, and long-term
130 time points, corresponding to ~1 month, 3-4 months, and 9 months after cell delivery (Figure 1
131 B). Our high-level goals were to: (i) elucidate the impact of hAMSC or iPSC-TM delivery on IOP;
132 and (ii) quantify the portion of IOP change due to changes in outflow facility, a key functional
133 metric of the TM. Outflow facility is the numerical inverse of the hydraulic resistance to aqueous
134 humor drainage through the conventional outflow pathway.

We expected transgenic MYOC$^{Y437H}$ mice to show elevated IOP by 6-7 months of age, when baseline IOP measurements were taken (9, 10, 26). Surprisingly, we saw no meaningful IOP difference between Tg-MYOCY437H mice (Tg group) vs. wild-type littermates (Figure 2; Table 1 and Table 2). Despite this lack of IOP elevation in the transgenic model, magnetically-steered delivery of hAMSCs led to a marked IOP decrease in Tg animals as compared to sham injection of saline at short-, mid-, and, long-term time points. The IOP reduction was sustained in hAMSC-treated eyes over all three time points, with no statistically significant difference between any combination of these time points. iPSC-TM treatment also led to a reduction in IOP compared to sham (phosphate-buffered saline, PBS) injection controls at both the short-and mid-term time points, although this difference did not reach statistical significance at the latter time. The IOP reduction due to iPSC-TM cells was approximately half that due to hAMSC treatment at both short- and medium-term time points (short term: $-4.3\,[-5.6, -2.9]\ \mathrm{mmHg}$ for hAMSC vs. $-2.3[-3.6, -1.0]\ \mathrm{mmHg}$ for iPSC-TM, $p = 0.021$; mid-term: $-4.5\,[-5.8, -3.1]\ \mathrm{mmHg}$ for hAMSC vs. $-1.9\,[-3.3, -0.4]\ \mathrm{mmHg}$ for iPSC-TM, $p = 0.005$; all data reported as means and 95% confidence intervals).

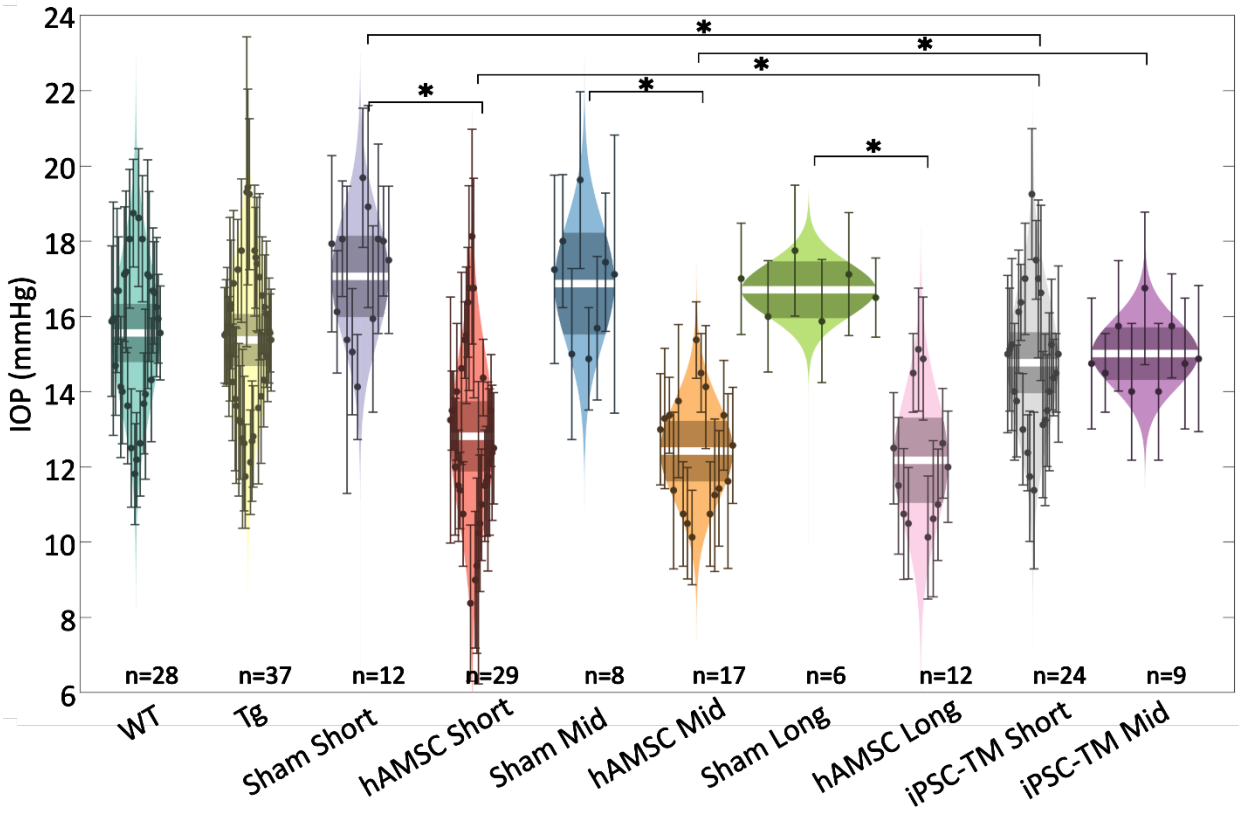


Figure 2. IOP was reduced by targeted cell delivery to the TM. In each experimental cohort, the central white strip indicates the mean, while the darker region represents the 95% confidence

interval on the mean. The colored region shows the distribution. Dots represent individual eyes, with error bars demarcating the 95% confidence intervals. For further information on experimental groups and statistical analysis refer to text. *$p < 0.05$ with Bonferroni correction (see Table 2). See below for a more complete statistical analysis. WT: wildtype hybrid mice (naïve control), Tg: Tg- MYOCY437H mice, Sham: Tg mice receiving saline injection, hAMSC: Tg mice receiving magnetically-steered hAMSCs, iPSC-TM: Tg mice receiving magnetically-steered iPSC-TMs. “Short”, "Mid”, and “Long” refer to time points. n is number of eyes measured in each group.

We observed increases in outflow facility for eyes receiving stem cells which were consistent with observed changes in IOP (Figure 3 A-B; Table 1 and Table 2). Specifically, no significant difference in facility was found between the naïve wildtype (WT) and transgenic groups, while hAMSC treatment led to a marked increase in outflow facility vs. injection (sham) controls at short-, mid- and long-term time points. Further, the percentage increases in facility due to hAMSC delivery vs. sham injection controls were similar at all time points. Groups receiving iPSC-TMs also showed an increase in facility, but these differences did not reach statistical significance. Specifically, hAMSC delivery led to a significantly higher percentage increase in facility compared to iPSC-TM delivery (short-term: $170\ [70, 310]\%$ for hAMSC vs. $40\ [-10, 110]\%$ for iPSC-TM, $p = 0.011$; mid-term: $180\ [110, 280]\%$ for hAMSC vs. $40\ [0, 110]\%$ for iPSC-TM, $p = 0.003$; data reported as percent increase in treatment group compared to relevant (sham) injection control).

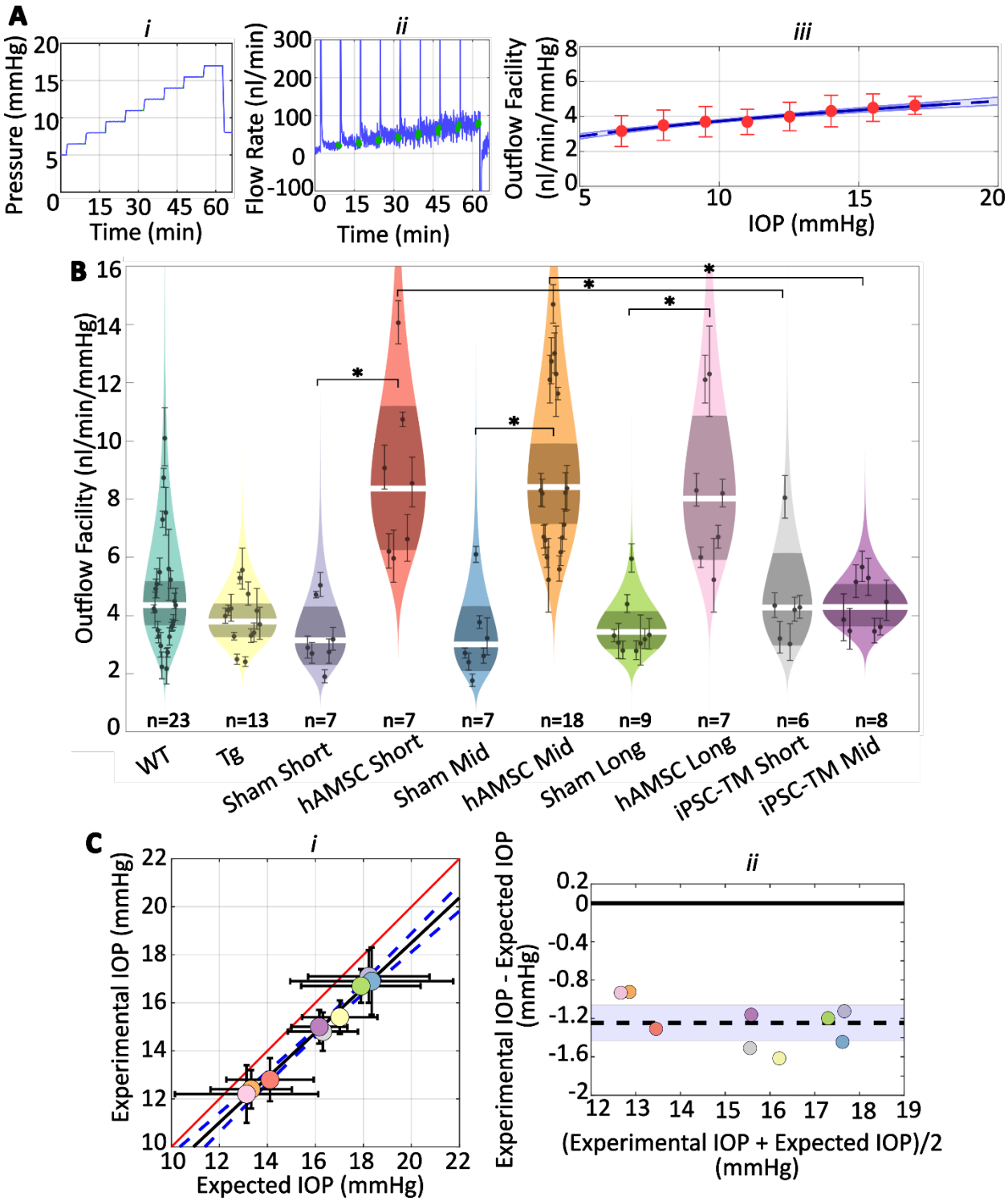


Figure 3. hAMSCs increase outflow facility in mice. **A** i-ii) IOP and flow rate vs. time for multiple pressure steps during the perfusion experiment in a representative eye. After each pressure step, the perfusion system automatically waits for a steady state inflow rate to be achieved, based on the criterion that the rate of change in the inflow rate falls below 3 nl/min/min. The steady intervals for each step are shown in green. Data has been trimmed to not include preparatory and pre-

loading phases. **A** iii) Calculated outflow facility (red dots) vs. IOP. The solid curve shows the fitted model with the shaded region being the 95% confidence interval on the regression line. Error bars are 95% confidence intervals on individual steps. **B)** Outflow facilities across different experimental cohorts. Refer to Figure 2 for interpretation details. Note that outflow facilities in mice follow a log-normal distribution. **C)** Cross-validation of experimentally-measured and expected IOP, calculated from measured facility values. i) Regression plot of experimental vs. expected IOPs. Solid black fitted line ($y = 0.94x - 0.21,\ R^2 = 0.99$) is shown along with its confidence bounds in dashed blue. Error bars show 95% confidence interval on both experimental (vertical) and expected (horizontal) IOPs. The unity line is shown as a solid red line. ii) Bland-Altman plot of IOP residuals (experimental minus expected IOPs) vs. average of experimental and expected IOPs. Individual experimental groups are indicated by colors matching those in panel B. Dashed line is shows the mean and is shown along with its 95% confidence interval (shaded). Solid line shows zero difference between the two parameters, i.e. the null hypothesis. For further information on experimental groups and statistical analysis refer to text. $*\ p < 0.05$ with Bonferroni correction (see Table 2).

We then asked whether the measured decreases in IOP were quantitatively consistent with the experimentally-measured increases in outflow facility. To answer this question, we used the modified Goldmann equation *(27)*, which relates IOP to facility and other variables, computing an "expected" IOP from the facility measurements for each cohort of mice. Comparison of this expected IOP with the actual (measured) IOP showed a close correlation (Figure 3 C*i*), determined by linear regression (slope of fitted line was not statistically different from one, $p = 0.22$, $R^2 = 0.99$). Still, the outflow facility measurements overestimated the actual IOP by a small amount ($1.2\ [1.1, 1.3]\ \mathrm{mmHg}$, $p < 10^{-6}$, null hypothesis: average difference between experimental and expected IOPs equals zero, Figure 3 C*ii*). Despite this "shift" between the experimentally-measured and expected IOP, the horizontal error bars in Figure 3 C*i*, derived by a propagation of error analysis, include the unity line for all groups, suggesting that the small discrepancy between the two experimental and expected values falls within the measurement errors (see Discussion).

*b. Cell delivery increased TM cellularity*

The observed reductions in IOP and increases in outflow facility after delivery of both cell types suggested functional changes in the conventional outflow pathway. We therefore asked whether these changes were associated with alteration of the cellular density in the TM by evaluating cell counts in histological sections of the iridocorneal angle from all of our experimental groups (Figure 4; Table 1 and Table 2). We observed more nuclei in eyes receiving cell transplantation, with a striking 2.2-fold increase in TM cellularity (normalized to the anterior-posterior length of the outflow tissues) after hAMSC treatment at the short-term time point vs. the corresponding (sham) injection control (Figure 4 C). Interestingly, this spike in TM cell density was followed by a decline over time, reaching a 1.6-fold increase at the mid-term time point, and apparently plateauing at

214 1.6-fold at the long-term time point. Despite this modest decline, hAMSC-treated eyes showed
215 significantly higher cellular density vs. their injection controls at both mid-term and long-term time
216 points.

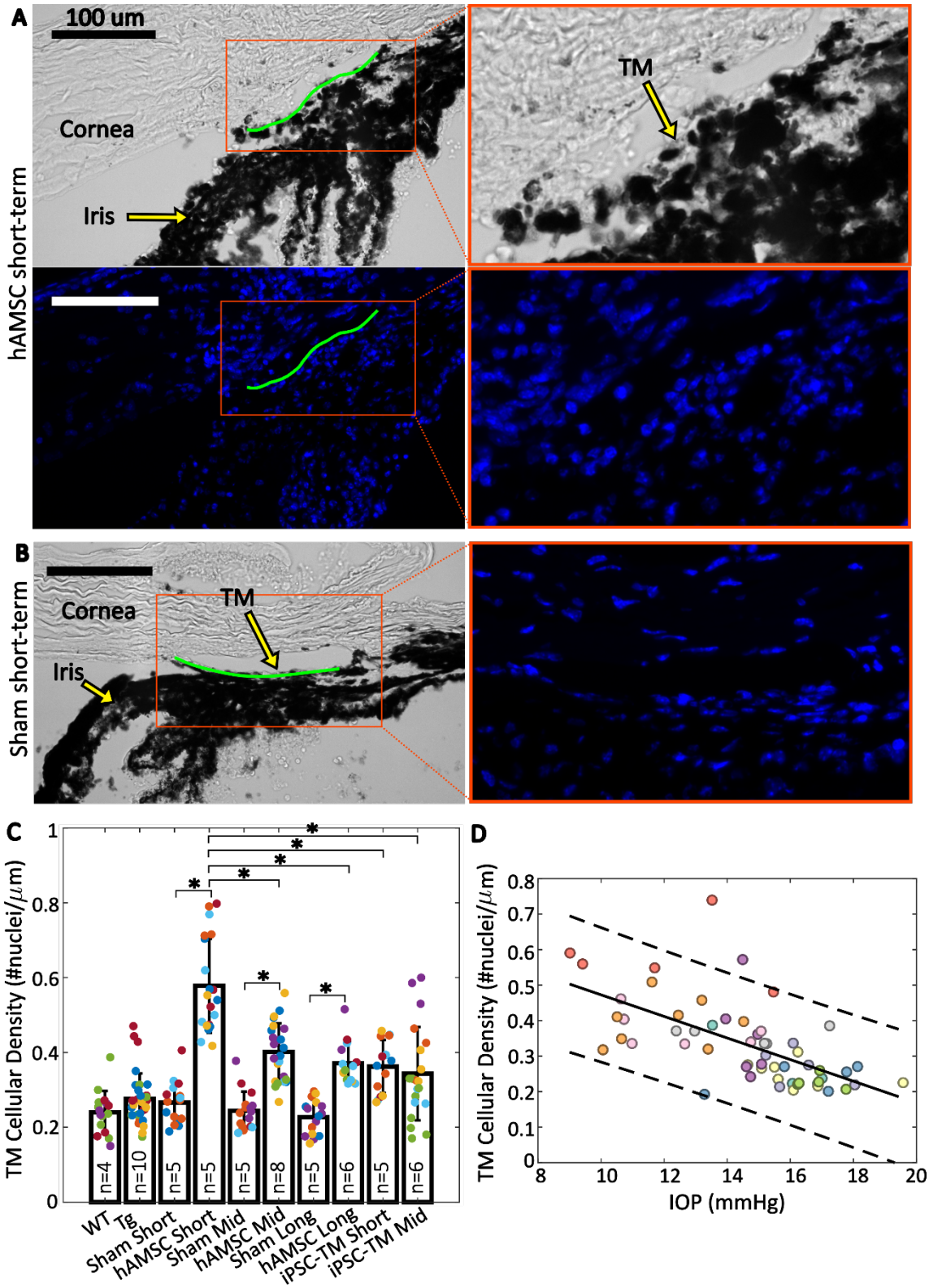


Figure 4. TM cellular density is improved by stem cell delivery. **A** and **B)** Brightfield and fluorescent micrographs of the irideocorneal angle (sagittal view) taken from a representative eye from the iPSC-TM short-term **(A)** and sham short-term **(B)** experimental groups. Green line shows the

contour of the TM along the inner wall of Schlemm's Canal used for normalizing nuclei count. DAPI-stained nuclei in the fluorescent image are shown in blue. Adjacent panels show a magnified view of the angle. **C)** Comparison of TM cellular density (number of nuclei per length of inner wall of Schlemm's canal) for various experimental cohorts. Bars show mean and standard deviation. Multiple sections analyzed from each eye are coded with the same color. n = number of eyes. Linear mixed-effect model, *$p < 0.05$ with Bonferroni correction (see Table 2). **D)** Cross-comparison of TM cellularity vs. IOP for the eyes shown in panel **C**. The negative correlation between the variables was statistically confirmed (Pearson correlation coefficient = $-0.63$ and $p < 10^{-7}$). Each color represents one eye, with different colors matching the experimental groups shown in Figure 2. Trend line (solid) is shown along with the 95% prediction interval (dashed).

Delivery of iPSC-TMs also led to an increase in TM cellular density vs. (sham) injection controls at both short-term and mid-term time points, although these differences were more modest than seen in hAMSC-injected eyes and did not reach statistical significance. Interestingly, the TM cellular densities in iPSC-TM-treated eyes at both time points were comparable to those at the mid-term and long-term time points in hAMSC-treated eyes but were significantly different than hAMSC-treated eyes at the short-term time point.

Cross-plotting normalized TM cellularity vs. IOP for pooled data from all the experimental groups (Figure 4D) showed a strong negative correlation between these two parameters, indicating an association between greater TM cellularity and lower IOP.

*c. hAMSC transplantation significantly decreased basement membrane material*

An increased deposition of extracellular matrix (ECM), and in particular basement membrane material (BMM), in the TM immediately adjacent to the inner wall (IW) of Schlemm's canal has been associated with ocular hypertension *(28, 29)*. Since this region within the TM accounts for the majority of AH outflow resistance *(30)*, we asked whether the amount of BMM was altered by stem cell treatment. To address this question we compared the mid-term hAMSC transplanted group vs. its corresponding injection control (Figure 5), selecting the mid-term time point for this analysis since this was the longest time point previously studied *(10)* and we were interested in persistent ECM changes within the TM.

Reduced amounts of BMM adjacent to the inner wall of Schlemm's canal were evident in transmission electron micrographs from eyes receiving hAMSCs compared to sham-injected controls at the mid-term time point (Figure 5A). Quantification showed that stem cell treatment significantly decreased the amount of BMM, as determined by the ratio of BMM length adjacent to Schlemm's canal inner wall to total inner wall length; specifically, this ratio was 0.52 [0.34, 0.70]

in sham-treated eyes vs. 0.34 [0.22, 0.47] in hAMSC-treated eyes ($p < 0.0001$). The BMM length ratio was measured by two independent annotators (MRB, CRE), and differences between the annotators were not significant (annotator considered as a random effect, $p \approx 1$, likelihood ratio test).

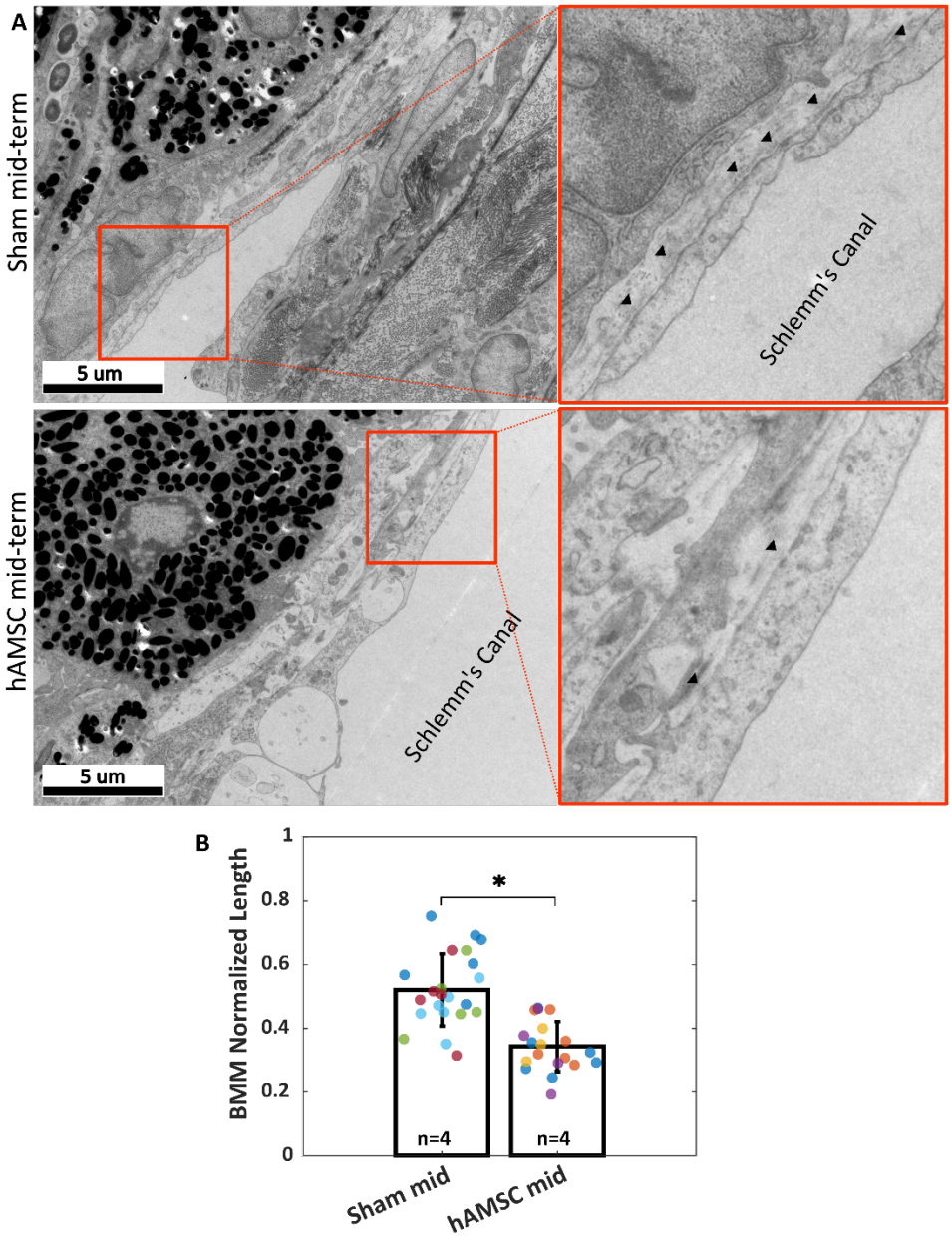


Figure 5. Ultrastructural analysis of ECM underlying the inner wall of Schlemm's canal (basement membrane material, or BMM). A) Greater amounts of BMM are evident immediately adjacent to the inner wall of Schlemm's canal (arrowheads) in a saline-injected eye (top row) vs. in a hAMSC-treated eye (bottom row) at the mid-term time point. The images at right are a zoomed view of the orange boxed areas in the left panels. B) The normalized length of BMM directly in contact with

265 the IW (length of BMM material divided by length of inner wall of Schlemm's canal) for the
266 experimental groups represented in panel A. Dots represent the average value between
267 annotators for each measured section. Multiple sections analyzed from each eye are coded with
268 the same color. n = number of eyes. Linear mixed-effect model. $*\, p < 0.05$.

269 *d. Exogenous cells were retained for multiple weeks in the TM*

270 Manuguerra-Gagné et al. previously reported a surprisingly low retention duration of hAMSCs in
271 the TM of rat eyes, with virtually no fluorescently-labeled exogenous cells being present in
272 histological sections four days after injection *(6)*. We therefore pre-labelled injected cells with
273 PKH26 fluorescent dye, which allowed us to track cells for up to 3 weeks after injection. *En face*
274 images showed a relatively uniform distribution of cells over the entire circumference of the eye
275 (Figure 6A), similar to previous results with magnetically steered cells *(15)*. Sagittal sections
276 (Figure 6B) showed an accumulation of exogenous cells deep within the iridocorneal angle.
277 Interestingly, strong fluorescent signals were observed within the TM in iPSC-TM-injected eyes,
278 indicating cell integration with the target tissue; in contrast, most hAMSCs accumulated close to
279 the TM (within $\sim 50\ \mu m$), but did not enter the TM. Note that fluorescent signals observed in the
280 posterior part of the eye and outside the eye near the limbus were caused by autofluorescence
281 (Supplementary Figure 3).

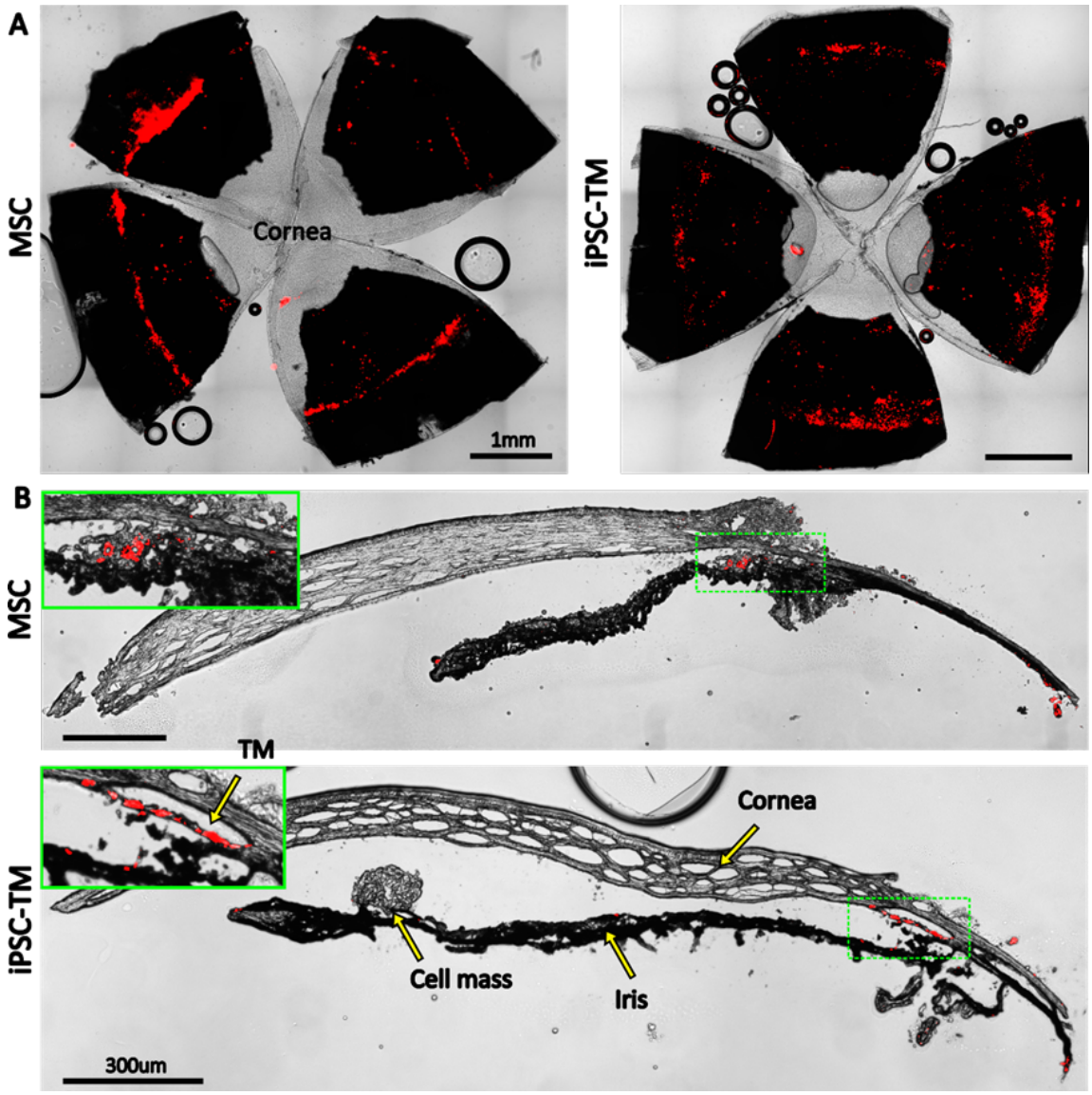


Figure 6. Retention of exogenous cells in the anterior segment 3 weeks after injection. Distribution of both hAMSC and iPSC-TM cells (red) are shown in A) *en face* images of the anterior segments and B) sagittal sections. In panel B), insets show a magnified view of the sites with the most intense fluorescent signal (green boxes). Autofluorescence can be seen in the posterior chambers as well as exterior to the corneoscleral shell. A cell mass, possibly a growing tumor, can be seen over the iris in the iPSC-TM injected eye.

*e. iPSC-TM transplantation led to significant incidence of tumor formation*

Unfortunately, there was a very high rate of tumorigenicity in eyes receiving iPSC-TMs, with more than 60% of eyes showing large intraocular masses within a month of cell injection, typically on the iris (Figure 6B). In most cases these tumors left the eyes unusable for IOP or outflow facility measurements. Examination of select iPSC-TM-transplanted sections by a board-certified

294 pathologist (HEG) confirmed the presence of tumors (Figure 7), based on observation of rosettes
295 and neuroectodermal phenotype, characteristics also found in various tumor types, including
296 retinoblastoma *(31)*. Additionally, a high nuclear-cytoplasmic ratio, a hallmark of tumor
297 malignancy *(32)*, and rarefaction due to tissue necrosis were noted. No signs of tumor growth
298 were observed in the eyes injected with hAMSCs at the long-term time point (Figure 7).

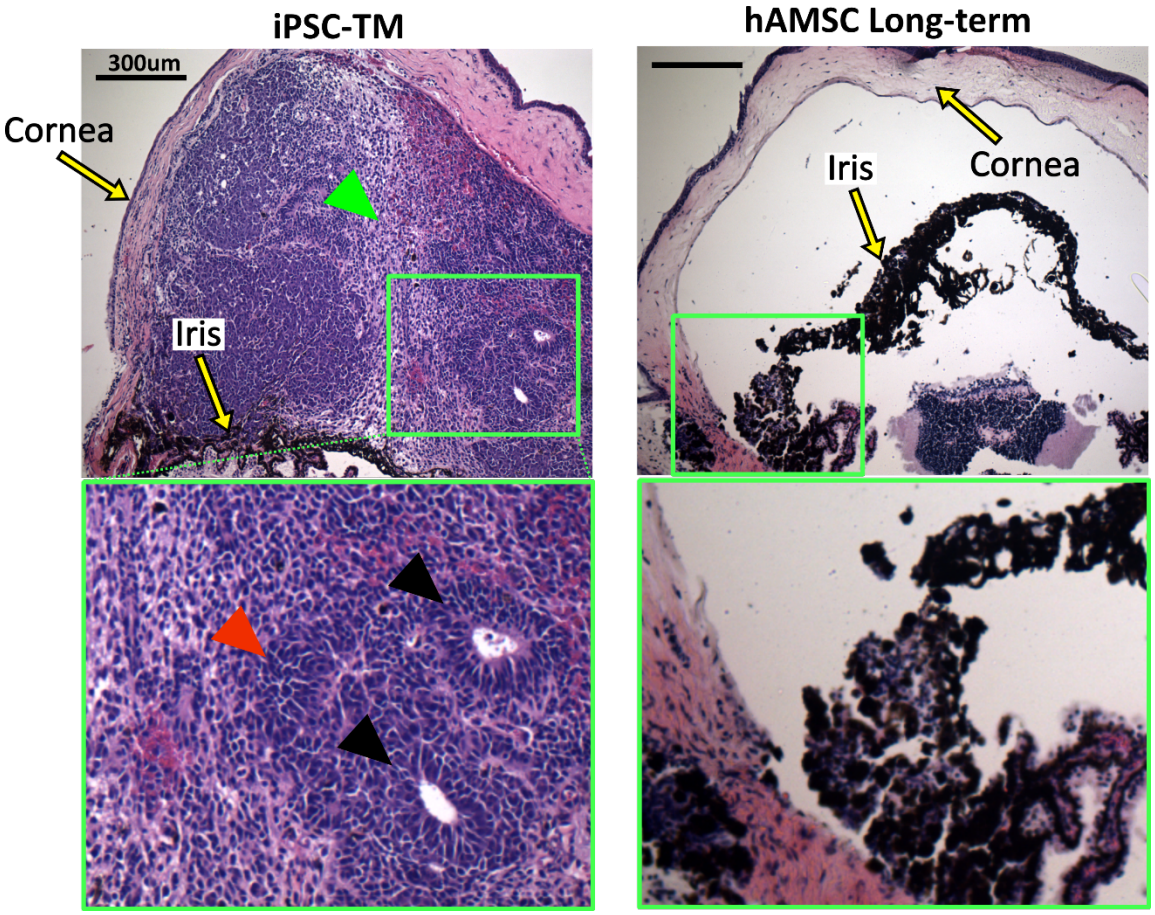


299

300 Figure 7. Histopathological assessment of tumors in eyes receiving transplanted cells. iPSC-TM-
301 and hAMSC-transplanted eyes were stained with hematoxylin and eosin (H&E). iPSC-TM
302 sections show distinct tumor characteristics in the anterior chamber, including the presence of
303 rosettes (black arrowheads), densely packed cells with high nuclear-cytoplasmic ratios (red
304 arrowhead), and more loosely coherent cells (green arrowhead). Note that eyes were collected
305 immediately after showing visible signs of tumor growth (usually within a month post-
306 transplantation) and not at a pre-defined time point. hAMSC eyes at long-term time point showed

307 no sign of tumor growth. In all panels, the green boxes provide a magnified view of the areas
308 where tumor growth or the accumulation of exogenous cells occurred.

309 **4. Discussion**

310 The overarching goal of this study was to evaluate the effectiveness of a magnetic TM cell delivery
311 technique we previously developed *(15)*. Specifically, by delivering stem cells into the eyes of a
312 mutant myocilin mouse model of POAG and observing the effects on IOP and aqueous humor
313 dynamics for an extended period of time, we wished to evaluate the potential of this treatment for
314 eventual clinical translation *(33)*. We hypothesized that our targeted magnetic delivery approach
315 would prove efficacious. A secondary goal was to compare the efficacy of two clinically relevant
316 stem cell types: human adipose-derived mesenchymal stem cells (hAMSCs) and iPSCs that had
317 been differentiated towards a TM cell phenotype (iPSC-TMs).

318 *a. hAMSC delivery led to long-term IOP reduction*

319 Our major finding was that magnetically steered delivery of hAMSCs led to a significant and
320 sustained lowering of IOP, which could be almost entirely explained by improved function of the
321 conventional outflow pathway. Specifically, we saw a ~27% (4.5 mmHg) IOP reduction in eyes
322 receiving hAMSCs vs. saline (sham) injection control eyes, which was sustained for 9 months
323 after cell delivery. This lowering of IOP was closely related to a stable ~2.8-fold increase in outflow
324 facility in the hAMSC treatment group vs. saline injection controls.

325 Eyes subjected to saline injection exhibited marginally higher IOPs and lower outflow facilities on
326 average, in comparison to the transgenic animals at baseline. However, due to the lack of
327 statistical significance in these differences and the inherent age difference between the saline-
328 injected animals and the non-injected controls at baseline, no conclusive inference can be drawn
329 regarding the effect of saline injection. To investigate this phenomenon further, we also analyzed
330 IOPs in uninjected contralateral eyes at the mid-term time point (Supplementary Tables 1 and 2,
331 Supplementary Figure 4). The uninjected contralateral transgenic eyes (10 months old) showed
332 an IOP of 16.5 [15.9, 17.1] mmHg, which was intermediate between the IOP levels of the 6–7-
333 month-old Tg group (15.4 [14.7, 16.1] mmHg) and the sham-injected group (16.9 [15.5, 18.2]
334 mmHg). However, none of these differences reached statistical significance. Of note, contralateral
335 hypertension has been previously reported after subconjunctival and periocular injection of
336 dexamethasone-loaded nanoparticles *(34)*, and we similarly cannot definitively rule out potential

contralateral effects induced by our stem cell injections. Thus, we cannot draw any definite conclusions from these additional IOP comparisons at this time.

Our measured IOPs were close to “expected IOPs” calculated from facility measurements, strongly suggesting that the majority of the IOP lowering effect after hAMSC delivery was due to an improvement in the function of the conventional outflow pathway.

*b. There was a slight offset between measured and expected IOPs*

Despite the very close correlation between measured and expected IOPs noted above, there was a small but consistent offset between these two quantities, which may be due to several factors. First, cell delivery could theoretically cause a decrease in the rate of AH formation or an increase in the rate of uveoscleral outflow, which would lower experimentally-measured IOP. However, according to Equation 2, a change in the pressure-independent flow rate ($Q$) would disproportionately affect the IOP in groups with lower facility. For example, if we conservatively assume that the 1.2 mmHg average residual (Experimental IOP − Expected IOP) was caused by a difference in inflow rate for transgenic animals vs. wild-type animals, which we used as the reference for calculating inflow rate (see Methods), the 95% confidence interval on the mean of the residuals would have been ~5 times larger than what we actually calculated. The second possible explanation is that the mismatch was caused by an error in rebound tonometry, for example due to tonometer miscalibration or an anesthesia-induced drop in IOP *(35)*. However, if we assume that all groups, including WT animals, had an experimentally-measured IOP that was artifactually lower than true IOP, the pressure-independent flow rate ($Q$) calculated for WT animals would incorporate this effect. Thus, when this $Q$ is used to calculate expected IOPs for groups other than WT animals, there should not be an offset between the experimental and expected IOPs, at least for groups with facilities similar to WT animals. We therefore suggest that the most plausible explanation is an inherent difference between the transgenic and WT animals, such as in the biomechanical properties of the cornea (leading to an error in the IOP read by the tonometer), in the episcleral venous pressure, or in the amount of IOP reduction due to anesthesia.

Despite some uncertainty about the minor offset between the expected and measured IOPs, the data strongly suggests that the IOP lowering caused by stem cell therapy is largely due to a restoration of function to the conventional outflow pathway.

367 *c. hAMSC treatment led to increased TM cellularity and reduced BMM*

368 One of the hallmarks of POAG is loss of TM cells *(5)*, which was an early motivation for TM cell
369 therapy as a potential treatment for this disease. We found that hAMSC delivery led to a striking
370 2.2-fold increase in TM cellularity 3-4 weeks after treatment vs. saline-injected controls, which
371 showed cellularities similar to eyes from WT mice. This increased cellularity declined somewhat
372 by 3-4 months after cell injection, but then stabilized for up to 9 months after injection. Additionally,
373 the increase in cellularity was strongly correlated with a decrease in IOP for pooled data from all
374 the experimental groups. This correlation more directly highlights the potential of TM cell therapy
375 in treating ocular hypertension, where TM cellularity is reduced and IOP is elevated *(5)*.
376 Interestingly, Alvarado et al. showed that humans at birth have ~2.3-fold higher TM cellularity
377 compared to a 40 year-old individual, and that this cellularity reduces sharply within the first five
378 years of life *(5)*. This trend in human eye cellularity resembles, both qualitatively and
379 quantitatively, our observations after hAMSC treatment when the ~27-month average lifespan
380 *(36)* of the mouse is taken into account. Further studies of factors controlling TM cellularity after
381 hAMSC delivery are indicated but lie beyond the scope of the current study.

382 Another feature of POAG is an accumulation of ECM within the juxtacanalicular tissue *(37)*. The
383 mechanism(s) underlying this ECM accumulation are not entirely understood. Nevertheless,
384 increased levels of transforming growth factor-β2 (TGF-β2) in the AH of POAG patients *(38)* and
385 its role in decreasing the activity of matrix metalloproteinases (MMPs) suggest that the abnormal
386 ECM deposits may be due to decreased ECM turnover *(37, 39)*. Thus, after detecting the
387 significant increase in TM cellularity and reduction in IOP using hAMSCs, we wondered whether
388 transplanted cells would also affect ECM levels in the TM. Our quantification showed that this was
389 indeed the case: hAMSC-transplanted eyes at the mid-term timepoint had 35% less basement
390 membrane material (BMM) under the inner wall of Schlemm's canal than in saline-injected control
391 eyes. This finding is consistent with the general theme of TM functional restoration seen
392 throughout this study. A future study to analyze the levels of TGF-β2 in the AH as well as the ratio
393 of active to pro-form levels of MMPs in hAMSC-transplanted eyes would be of interest to better
394 understand the mechanism through which exogenous cells modulate ECM turnover.

395 *d. Comparison with previous work*

396 Unfortunately, it is not feasible to directly compare the results of this study with those of previous
397 studies that have successfully demonstrated the efficacy of non-magnetic cell therapy in

398 MYOC$^{Y437H}$ mice *(9, 10)*. This is due to the unexpected lack of a POAG phenotype in our
399 transgenic mice (discussed in detail below). Yet in our study, we found a stable IOP lowering and
400 increase in outflow facility over 9 months (corresponding to one-third of the animals' lifespan)
401 which for the first time attests to the possible longevity of IOP lowering due to TM cell therapy. In
402 addition, because of the targeted nature of our delivery technique, we could achieve these
403 reported therapeutic outcomes by injecting a total of only ~1,500 cells, which is significantly lower,
404 i.e. more efficient, than the 50,000 cells used in previous studies *(9, 10)*.

405 One literature comparison that can be made is for BMM normalized length. Li et al. reported
406 values of 0.40 [0.23, 0.57] for this quantity in naïve eyes and 0.50 [0.38, 0.60] for sham-injected
407 (PBS containing non-conjugated polymeric nanoparticles) eyes in 2-3 months old C57BL/6
408 mice*(28)*. Overby et al. measured a BMM normalized length of 0.29 [0.16, 0.42] in 6-7 month old
409 mice from the same strain *(29)*. Despite our sham mid-term group being 9-11 months old and
410 being on a transgenic background, with no phenotypic manifestation, the 0.52 [0.34, 0.70] BMM
411 normalized length we measured for this group is consistent with those previously reported values.
412 The fact that we observed reduced BMM length in cell-treated eyes vs. control values may
413 suggest that a homeostatic balance in cell-treated eyes was tipped towards the presence of less
414 BMM, consistent with hypotensive IOP measurements and greater outflow facility.

415 *e. hAMSCs outperformed iPSC-TMs*

416 This study for the first time compared the IOP-lowering performance of hAMSCs vs. iPSC-TMs –
417 two of the most clinically relevant cell types for future TM cell therapy *(33)*. Surprisingly, we found
418 that the performance of iPSC-TMs was significantly inferior to that of hAMSCs, as quantified by
419 several outcome measures; most notably, the IOP reduction after iPSC-TM cell delivery was only
420 half that seen after hAMSC delivery. The beneficial effect of iPSC-TM treatment on TM cellularity
421 was also significantly lower than hAMSC at the short-term time point (1.4-fold vs. 2.2-fold
422 increase), although this difference declined at the mid-term time point (1.4-fold vs. 1.6-fold
423 increase). In addition to their IOP-reducing efficacy, another major drawback of the iPSC-TMs
424 was the high incidence of ocular tumorigenicity. More than 60% of the eyes injected with iPSC-
425 TM cells developed tumors, requiring termination of the experiment. A body of previous literature,
426 including a systematic review of 1000 clinical trials involving mesenchymal stem cell
427 transplantation, finds no incidence of tumorigenicity in tissues receiving mesenchymal stem cells,
428 suggesting an intrinsic resistance to tumor formation once positioned in the correct niche *(18, 19)*.
429 On the other hand, tumorigenicity remains a concern for iPSC-derivatives due to transfection with

430 oncogenic factors, genetic aberrations during *in vitro* cultures, and contamination of transplants
431 with undifferentiated cells *(40–42)*. Despite following a protocol to isolate differentiated iPSC-TM
432 cells, including using a non-integrating viral vector for transfection of reprogramming factors and
433 a commonly-used magnetic activated cell sorting approach *(42)*, there unfortunately remains a
434 chance for contamination and reprogramming of these cells post-transplantation. Interestingly,
435 the iris is reported to be a favorable location for organ culture and tumor formation, with 5-fold
436 faster growth compared to subcutaneous injection, and thus has previously been considered for
437 tumorigenicity safety studies, emphasizing the importance of rigorous iPSC processing in any
438 future treatments involving iPSC-TM cell injection into the anterior chamber *(43–45)*.

439 *f. Cell retention profiles differed between the two cell types*

440 Both cell types were detectible in the anterior chamber three weeks after injection (Figure 6B),
441 with iPSC-TM cells tending to better integrate with the TM tissue whereas the hAMSCs mostly
442 accumulated close to, but not within, the TM. This phenomenon, which was consistently observed,
443 may be due to the widely-reported aggregation of mesenchymal stem cells immediately post-
444 transplantation *(46)*, which consequently prevented them from entering the deeper aspects of the
445 TM, characterized by narrow flow channels. Note that the exogenous iPSC-TMs more directly
446 contributed to increasing TM cellularity than did the hAMSCs due to the better integration of iPSC-
447 TM cells into the TM. This finding complicates the interpretation of the relationship between
448 increased TM cellularity and IOP reduction. In addition, loss of signal in long-term *in vivo*
449 fluorescent cell tracking is inevitable *(47)* so the fluorescent signal in Figure 6 may not be marking
450 all the exogenous cells retained in the anterior eye.

451 *g. A likely role for paracrine signalling underlying TM cell therapy*

452 The lack of specific hAMSC homing into the TM also provides important insight about the putative
453 mechanism(s) by which these cells lowered IOP and improved aqueous humor dynamics. Several
454 hypotheses address how injected cells may affect TM functional restoration: exogenous cells can
455 either integrate with the TM and differentiate into TM-like cells, or can promote endogenous TM
456 cell proliferation through direct contact or through their secretome. Du and colleagues, in two
457 studies using mice, showed that TMSCs that reach the TM co-express AQP1 and CHI3L1,
458 indicative of their differentiation into TM cells, although quantification was not performed *(11, 14)*.
459 Zhu et al. reported a 114% increase in TM cellularity after iPSC-TM injection in $MYOC^{Y437H}$ mice
460 compared to saline-injected controls, yet TM-residing exogenous cells accounted for only 23% of

461 this increase *(9)*. This finding is consistent with several studies that report the proliferative effect
462 of exogenous cells on the TM in terms of higher Ki-67 expression and BrdU signal, as well as an
463 increased prevalence of Nestin+ progenitor cells *(6, 9, 12)*. How this proliferation is mediated,
464 however, is a matter of controversy. In two studies, Zhu et al. showed that iPSC-TMs induce
465 significant proliferation of both cells from the TM5 cell line (an immortalized TM cell line) or primary
466 TM cells carrying Ad5RSV-myocilinY437H when in co-culture, yet did not when they were co-
467 cultured in the presence of a physical (membrane) separation between iPSC-TMs and TM cells
468 *(9, 12)*. Interestingly, Xiong et al. conducted similar experiments with TMSCs and MyocY437H
469 primary TM cells and observed no proliferative effect with or without contact between the cells
470 *(14)*. On the contrary, two studies have reported the beneficial effect of injecting conditioned
471 media from bone marrow MSCs in hypertensive rat eyes, including a significant reduction in IOP,
472 neuroprotection, and elevated proliferation markers in the TM *(6, 7)*. In our study, the significant
473 lowering of IOP seen after delivery of hAMSCs and their accumulation near, but not within, the
474 TM supports the notion that injected cells act upon the TM through their secretome. Thus, a
475 proteomic comparison of the secretome of hAMSCs and iPSC-TMs may provide significant insight
476 into their paracrine effect on TM functional restoration.

477 *h. Limitations*

478 The main limitation of this study was the lack of a POAG phenotype in our transgenic mouse
479 colony. Even though $MYOC^{Y437H}$ mice have previously been shown to exhibit an elevation in IOP
480 and a decrease in both outflow facility and TM cellularity, our colony did not show any difference
481 in those parameters compared to WT animals. While we are not certain of the cause, one
482 possibility is that our IOP measurements were inaccurate. However, this is unlikely because of
483 the correlation between measured IOP and outflow facility in cohorts (Figure 3C) and the fact that
484 IOPs in our wild-type animals lay within previously reported ranges *(9, 10, 29, 48)*. It should be
485 noted that reported IOPs for anesthetized WT C57BL/6 mice vary depending on the measurement
486 method used, with a lower bound of ~12.5 mmHg under deep levels of injection-induced
487 anesthesia *(49)* and an upper bound of ~20 mmHg under gas-induced extra light anesthesia *(28)*,
488 with values close to our measurements being frequent in the literature. An alternative, and
489 perhaps more likely, possibility is that the transgene was silenced in the original breeders of this
490 colony. Unfortunately, this only became evident after the 6-7 month wait time required for the
491 expected onset of the phenotype. Despite the strong effectiveness of our novel TM cell therapy
492 technique (even in the absence of ocular hypertension), the main concern is whether cell therapy
493 would work as effectively in a glaucomatous eye. Raghunathan et al. showed that when healthy

494 TM cells are cultured on the ECM derived from glaucomatous TM cells, the healthy cells
495 experience differential stiffening and altered expression profiles similar to the glaucomatous
496 phenotype *(50)*. Therefore, a glaucomatous ECM may negatively impact the exogenous cells and
497 curtail their therapeutic potential. Fortunately, since in our study hAMSCs did not seem to need
498 to integrate into the TM to lower IOP, they may also not be affected by glaucomatous changes in
499 the TM. Additionally, Goldmann's equation (Equation 2) shows that the same percentage increase
500 in outflow facility produces a greater magnitude of IOP lowering in a hypertensive eye vs. in a
501 normotensive eye. Therefore, evaluation of magnetically-steered hAMSC cell therapy in an
502 alternative pre-clinical glaucoma model is indicated.

503 An additional limitation is that, since histology was only performed on a subset of the eyes after
504 outflow facility measurements, it is possible that there may also have been undetected tumors in
505 the iPSC-injected eyes reported in the IOP and outflow facility plots. This could affect the reported
506 efficacy of the iPSC-TM cells, and further experiments comparing hADMSCs to more carefully
507 processed iPSC-TM cells may be worthwhile.

508 In summary, this work shows the effectiveness of our novel magnetic TM cell therapy approach
509 for long-term IOP reduction through functional changes in the conventional outflow pathway. The
510 comparison between hAMSCs and iPSC-TM cells strongly suggested the inferiority of the latter
511 cell type in this treatment paradigm, as judged by tumorigenicity and less effective IOP lowering.
512 The localization of injected hAMSCs deep in the iridocorneal angle, but not full integration into the
513 TM, supports the hypothesis that exogenous cells promote TM functional restoration through
514 paracrine signaling Therefore, even though the mouse model used in this study did not show a
515 POAG phenotype, this treatment approach merits further study with the eventual goal of clinical
516 translation.

517 **5. Materials and Methods**

518 *a. Experimental design*

519 We conducted experiments in several cohorts of mice, as follows:

520 - WT: wildtype hybrid mice (naïve controls)
521 - Tg: Tg-MYOCY437H mice, a model of POAG (see details below)
522 - Sham: Tg mice receiving phosphate-buffered saline (PBS, injection controls)
523 - hAMSC: Tg mice receiving magnetically-steered hAMSCs

524 • iPSC-TM: Tg mice receiving magnetically-steered iPSC-TMs

525 Our key outcome measures were IOP, outflow facility, TM cellularity, cell retention in the anterior
526 segment, and ultrastructural analysis of TM ECM, with timelines as indicated in Figure 1 B. All
527 measurements were made in *ex vivo* eyes, except for IOP, which was measured longitudinally in
528 living mice.

529 After breeding and genotyping, mice, regardless of sex, were maintained to age 6-7 months, when
530 transgenic animals were expected to have developed a POAG phenotype. We then made
531 baseline measurements and performed stem cell (or sham) injections, and followed animals for
532 various durations:

533 • Short-term: 3-4 weeks after cell injection
534 • Mid-term: 3-4 months after cell injection, and
535 • Long-term: 9 months after cell injection.

536 Exogenous cell retention in the anterior chamber was measured at only the short-term timepoint.
537 This is because in our experience (data not shown) the tracer's signal was only faintly present
538 two months after injection *in vivo,* while signal was maintained for a longer period *in vitro*, as
539 advertised by the manufacturer. We are unsure whether this loss of signal was caused by a loss
540 of cell integrity or by fluorescence fading *in vivo*. Further, due to the high incidence of
541 tumorigenicity and inferior overall effectiveness in animals receiving iPSC-TM cells, long-term
542 measurements as well as ultrastructural analysis were not pursued for this group. We chose to
543 perform ultrastructural analysis for hAMSC group at the mid-term time point, as this is the longest
544 timepoint previously studied *(10)* and enables comparison with previous work.

545 *b. Cell preparation*

546 hAMSCs were purchased commercially (Lonza Bioscience, Walkersville, MD) and were prepared
547 for injection as described previously *(15)*. The cells were maintained at 37° C and 5% $CO_2$ in α-
548 MEM supplemented by 10% FBS and 1% penicillin and streptomycin and 2 mM L-glutamine. Cells
549 were passaged using 0.05% trypsin (25-053-CI, Corning Inc., Corning, NY) to detach cells,
550 followed by resuspension and seeding at 5000 cells/$cm^2$ in T-25 cell culture flasks. hAMSCs at
551 80% confluence (passages 5 or 6) were magnetically labeled by overnight incubation with 150
552 nm amine-coated superparamagnetic iron oxide nanoparticles (SPIONs; SA0150, Ocean
553 NanoTech, San Diego, CA) at 25 µg/ml, followed by inspection under light microscopy to verify

554 sufficient SPION endocytosis. Cells were then trypsinized, resuspended by addition of cell culture
555 media, and placed in a 1.5 ml microtube. To remove insufficiently magnetized cells, a 0.25" cubic
556 N52 neodymium magnet was placed on the side of the tube, resulting in rapid formation of a cell
557 pellet close to the magnet. Supernatant and non-magnetic cells were then removed.

558 In exogenous cell retention studies, the cells remaining in the microtube were labeled using the
559 PKH26 lipophilic dye kit (Sigma-Aldrich, St. Louis, MO) according to the manufacturer's
560 instructions. In brief, a cell solution was prepared in the diluent component of the kit and was
561 vigorously mixed with an equal volume of the 4 μM dye solution. After 3 minutes at room
562 temperature, an equal volume of FBS was added to the cell solution to stop the reaction and cells
563 were washed 3 times with the cell culture media to remove any unbound dye. For all the
564 experiments where animals received hAMSC, cell count and >90% viability was verified using a
565 Countess II Automated Cell Counter (Thermo Fisher Scientific, Waltham, MA). The cells were
566 then resuspended in sterile PBS (1X, Thermo Fisher Scientific, Waltham, MA) to a final
567 concentration of 1 k cells/μl.

568 Mouse iPSC-TMs have previously been developed and characterized *(9)*. In brief, mouse dermal
569 fibroblasts are reprogrammed through Sendai virus-mediated reprogramming with the
570 transcription factors OCT4, SOX2, KLF4, and c-MYC. The pluripotency of reprogrammed iPSCs
571 was confirmed using RT-PCR, immunocytochemistry, immunoblotting, and teratoma formation.
572 iPSCs were then differentiated by culturing in conditioned media from primary human TM (phTM)
573 cells. To prepare this conditioned media, phTM cells were extracted from donor eyes and cultured
574 in α-MEM supplemented by 10% inactivated FBS and 2% primocin. Conditioned media was then
575 collected from the cells and sterilized by passing through a 0.2 μm membrane filter. The iPSCs
576 were maintained in conditioned media for 8 weeks to induce differentiation. It is important to
577 remove any undifferentiated iPSCs from the iPSC-TM populations due to the risk of tumorgenicity
578 associated with pluripotent stem cells. Therefore, the iPSC-TMs were incubated with CD15
579 antibodies (Miltneyi Biotec, Bergisch Gladbach, Germany) conjugated with magnetic microbeads
580 to label the undifferentiated iPSCs. Then the cells were washed, loaded into a MACS LD column
581 and were placed in a magnetic separator (Miltenyi Biotec, Germany).

582 *c. Transgenic mice*

583 All animal procedures were approved by the Georgia Tech Institutional Animal Care and Use
584 Committee and performed in conformance with the ARVO Statement for the Use of Animals in

585 Ophthalmic and Vision Research. Breeder pairs of C57BL/6 Tg-MYOCY437H mice were shipped
586 from Iowa to a quarantining facility (Charles River, Wilmington, MA, USA), underwent IVF
587 rederivation, and were shipped to Georgia Tech after ~4 months. Breeders carrying one copy of
588 the transgene on a C57BL/6 background were crossed with SJL mice (Charles River) of similar
589 age, with half of the hybrid offspring carrying the transgene. Pups were genotyped using human
590 MYOC primers (forward: CGTGCCTAATGGGAGGTCTAT; reverse:
591 CTGGTCCAAGGTCAATTGGT). Only F1 animals were used in studies.

592 *d. Cell injections*

593 Cell injection needles were fabricated as described previously *(15)*. In brief, glass micropipettes
594 were pulled using a pipette puller (P-97, Sutter Instruments, Novato, CA, USA) and the tips were
595 broken and beveled at a 30° on a microelectrode beveler (BV-10, Sutter Instruments, Novato, CA,
596 USA) followed by rotating to both sides for enhanced sharpness (tri-beveling). The resulting
597 needle had a pointed tip and an outer dimeter of approximately 100 μm. Cell adhesion to the
598 needle walls in the lumen can cause inconsistent cell delivery to the eye; thus, we plasma cleaned
599 the needles, coated them with trichlorosilane and loaded them with 0.02% Pluronic F-127 (P2443,
600 Sigma-Aldrich) for 1 hr at room temperature followed by vigorously rinsing with PBS. Needles
601 were sterilized with 70% ethanol prior to injections.

602 Each animal was prepared for unilateral injection of cells by applying a tropicamide eyedrop
603 (Bausch and Lomb, Bridgewater, NJ, USA) to start pupil dilation before inducing anesthesia using
604 an induction chamber receiving 2.5% isoflurane at 600 ml/min. Once toe-pinch reflex was lost,
605 the animal was transferred to a heated bed and the head was immobilized with Velcro straps
606 while anesthesia was maintained through a nose cone. A drop of tetracaine (Bausch and Lomb)
607 was applied to the eye being injected while the contralateral eye received ophthalmic lubricant
608 (SystaneUltra, Alcon, Geneva, Switzerland) to prevent drying. The needle, mounted on an injector
609 assembly (MMP-KIT, WPI, Sarasota, FL, USA), was attached to a micromanipulator and
610 connected to a microsyringe pump (PHD Ultra, Harvard Apparatus, Holliston, MA, USA). The
611 needle was filled with 3 μl of the injection solution (either cells, or PBS for control (sham)
612 injections), aligned at a 30° angle with the eye, and advanced into the AC in a swift motion until
613 the tip was located approximately in the center of the AC while the eye was held in a proptosed
614 position using a pair of non-magnetic forceps (Figure 1 A). A total of 1.5 μl of the solution was
615 injected at 2.4 μl/min and if the solution contained cells, a point magnet (a thin stainless-steel rod
616 attached to a permanent magnet) was used to magnetically steer the cells towards the TM in a

617 continuous motion for the duration of cell ejection from the needle as previously described in detail
618 *(15)*. Injected eyes received ophthalmic antibiotic combination ointment (neomycin, polymyxin,
619 bacitracin) and were kept on a heated bed until recovery from anesthesia.

620 *e. IOP measurements*

621 We measured the IOPs between 1 to 3 pm (to minimize diurnal variations) by first placing the
622 mouse in an induction chamber until the righting reflex was lost and breathing slowed. The animal
623 was then transferred to a heated platform, secured with straps, and a tonometer (TonoLab, iCare,
624 Vantaa, Finland) mounted on a micromanipulator (M3301, WPI, Sarasota, FL, USA) was aligned
625 perpendicular to the corneal surface at the center of the cornea. Eight IOP measurements were
626 taken from each eye and the reported IOP was the average of all 8 measurements. Even though
627 some labs exclude the highest and lowest of the 8 measurements from the IOP average *(51)*, we
628 did not observe a significant intra-measurement variability and thus included all the 8 replicates
629 when determining the IOP. The entire duration of IOP measurement was typically 3 minutes or
630 less, which is less than has been reported for the start of significant anesthesia-induced IOP
631 reduction *(35, 52)*.

632 *f. Measurement of outflow facility*

633 Outflow facility, which quantifies the ease of fluid drainage from the eye, is defined as the ratio of
634 steady-state outflow rate over intraocular pressure in an enucleated eye. We measured facility in
635 enucleated eyes using the previously established iPerfusion system *(53)*. The system's sensors
636 were calibrated before each measurement session to ensure reliability and the absence of
637 bubbles or leaks, which can cause large errors in the measurements. Animals were euthanized
638 by intraperitoneal injection of sodium pentobarbital and eyes were enucleated by sliding a pair of
639 fine angled forceps behind the eye through the nasal side of the eye socket and pulling the eye
640 out by grabbing onto the optic nerve and the surrounding retrobulbar tissues. The posterior of the
641 eye was secured to a mounting post using a very small drop of cyanoacrylate adhesive
642 (Superglue) inside a heated water bath (35°C) filled with DPBS supplemented with 5.5 mM
643 glucose. A beveled micropipette, mounted on a micromanipulator, was then used to cannulate
644 the eye at a 30° angle. The eyes were stabilized at an IOP of 8 mmHg for 30 minutes and then
645 perfused at 8 evenly distributed pressure steps starting from 4.5 mmHg and finishing at 16.5
646 mmHg while flow rate and pressure data were acquired (Figure 3 Ai-iii). The resulting flow-
647 pressure data were fit with an empirical power-law relationship *(53)*

$$C(P) = C_r \left(\frac{P}{P_r}\right)^{\beta} \quad (1)$$

648 where $C$ is the steady-state outflow facility calculated for each pressure step, $P$ is the steady state
649 pressure for that step, and the subscript $r$ refers to the parameter evaluated at the reference
650 pressure of 8 mmHg which corresponds to the physiologic pressure difference across the
651 conventional outflow pathway *(53)*. $\beta$ is a non-linearity parameter that is determined by data fitting
652 along with $C_r$. A total of 114 eyes were randomly chosen for outflow facility measurements, of
653 which, 9 were excluded due to failed perfusion (e.g., poor cannulation).

654 *g. Comparison between experimental and expected IOP*

655 Steady-state AH dynamics can be described by the modified Goldmann equation *(27)*:

$$Q = Q_{in} - Q_0 = C(IOP - P_e) \quad (2)$$

656 where $Q_{in}$ is the rate of AH humor formation, $Q_0$ is the uveoscleral (unconventional) outflow rate,
657 and $P_e$ is the episcleral venous pressure. Since the left-hand side of Equation 2 is essentially
658 pressure-independent, $Q$ was assumed to be the same across all the experimental groups.

659 To cross-validate the IOP and outflow facility measurements, we calculated $Q$ in wildtype animals
660 by inserting the mean measured outflow facility and mean measured IOP from wildtype animals
661 into Equation 2, assuming $P_e$ to be 7 mmHg *(53)*. Average outflow facilities for all the groups were
662 then adjusted using Equation 1 to account for the pressure-dependence of facility. Using these
663 adjusted facilities and assuming $Q$ to be the same for all groups, we calculated an "expected IOP"
664 for each experimental group, which can be interpreted as the IOP that is consistent with the
665 measured outflow facility.

666 *h. Histology, histopathology, and morphometric studies*

667 Similar to the procedure used previously *(15)*, all experimental eyes were immersion fixed in 10%
668 formalin (Fisher Healthcare, Waltham, MA, USA) overnight at 4°C after the corresponding *in vivo*
669 and *ex vivo* measurements (no measurements were performed on the eyes used for exogenous
670 cell retention study). Of these eyes, a total of 59 were randomly selected from various groups for
671 TM cellularity quantifications. Eyes were then dissected under a surgical microscope and isolated

672 anterior segments were cut into four leaflets. This anterior segment wholemount was placed on a
673 glass side with the cornea facing up and mounted with PBS. A Leica DMB6 epifluorescent
674 microscope (Leica Microsystems, Wetzlar, Germany) was used to create fluorescent *en face*
675 tilescan images. Two quadrants of each wholemount were then prepared for cryosectioning.
676 These quadrants received sequential 15 minute treatments in 15% sucrose (Sigma-Aldrich, St.
677 Louis, MO, USA), 30% sucrose, and a 1:1 solution of 30% sucrose and optimal cutting
678 temperature (OCT) media. After embedding in OCT, samples were floated in a 100% ethanol bath
679 cooled by dry ice to flash freeze. 10 µm-thick sagittal sections were cut using a CryoStar NX70
680 cryostat (ThermoFisher Scientific, Waltham, MA, USA) and placed on Superfrost gold plus slides
681 (ThermoFisher Scientific, Waltham, MA, USA). In an additional step, specific to TM cellularity
682 quantification, the samples were permeabilized with 0.2% Triton X-100 for 10 minutes and stained
683 with DAPI (NucBlue fixed cell DAPI, Invitrogen, Waltham, MA, USA) for 15 minutes followed by
684 coverslipping with antifade media (Prolong Gold antifade medium, Invitrogen, Waltham, MA,
685 USA). Sagittal sections were then imaged as tilescans.

686 To quantify TM cellularity, ideally all the cells in the TM should be counted. However, due to partial
687 or complete collapse of the Schlemm's canal and the small separation between the TM and the
688 iris in the murine iridocorneal angle *(54)*, identifying the boundaries of the TM can be challenging.
689 Thus, to minimize error, we instead counted the DAPI-stained nuclei in the region that we could
690 identify as the TM with a high confidence and normalized this count by the length of the inner wall
691 of Schlemm's canal adjacent to this segment (Figure 4 A). Note that morphological characteristics
692 such as the autofluorescence in the corneoscleral shell, high degree of pigmentation in the iris,
693 as well as the change in the density and orientation of the cells transitioning from the TM to iris
694 helped with locating the TM cell nuclei.

695 Eyes of animals injected with iPSC-TMs showing anatomical signs of tumor growth were
696 enucleated and immersion fixed in 10% formalin for histopathological studies. Three of these eyes
697 were randomly chosen, dehydrated, and embedded in paraffin. Subsequently, 5 µm thick sagittal
698 sections were cut using a microtome (ThermoFisher Scientific, Waltham, MA, USA) and stained
699 with hematoxylin and eosin (H&E). Three additional eyes from hAMSC long-term group
700 underwent the same procedure for comparison.

701 *i. Quantification of ECM underlying the inner wall of SC*

702 The amount of basement membrane material (BMM) in the hAMSC mid-term experimental group
703 and in corresponding injection control eyes (four eyes in each cohort) were quantified using
704 electron micrographs, using an approach similar to that previously described *(28, 29)*. In brief, the
705 two anterior segment quadrants not used for TM cell counting (described above) were immersion
706 fixed overnight at 4°C in universal fixative (2.5% glutaraldehyde, 2.5% paraformaldehyde in
707 Sörensen's buffer). The specimens were next embedded in Epon resin, and 65-nm sagittal
708 sections were cut through iridocorneal tissues using an ultramicrotome (Leica EM UC6, A-1170;
709 Leica Mikrosysteme GmbH) followed by staining with uranyl acetate/lead citrate. Sagittal sections
710 were examined with a JEM-1400 electron microscope (JEOL USA, Peabody, MA) at 8000x
711 magnification. At least one section per quadrant was included in the quantification of basement
712 membrane material (BMM) deposits as described below.

713 The lengths of BMM segments directly in contact with the inner wall of Schlemm's canal (IW) and
714 the total length of IW were measured from electron micrographs using ImageJ *(55)*by two
715 independent annotators in a masked fashion. To enhance BMM identification from micrographs,
716 we first adjusted the contrast for each image, using an ImageJ macro that assigned a brightness
717 level of 255 to a manually-selected region of the lumen of SC and a brightness level of zero to a
718 manually-selected region of a cell nucleus. The ratio of the length of BMM segments directly
719 underlying the IW to the total length of IW was calculated for each segment, representing the
720 extent of non-fenestrated BMM material underlying the IW. Supplementary Figure 1 exhibits an
721 example of the demarcations. Note that ECM deposits clearly separated from the IW were not
722 considered as BMM deposits.

723 *j. Statistical analysis*

724 IOP, outflow facility, and TM cellularity index were tested for normality using the Shapiro-Wilk test
725 for each treatment group. Since outflow facility is known to be log-normally distributed *(53)*, facility
726 data was first log-transformed prior to conducting any statistical tests. All outcome measures,
727 except for TM cellularity and normalized BMM length, were analyzed by one-way ANOVA. For
728 TM cellularity and BMM length, we used a linear mixed-effects model, treating the experimental
729 group as the fixed effect while considering the eyes, various sections of each eye, and annotators
730 (for BMM only) as replicates, i.e. as random effects. Following these analyses, we conducted *post*
731 *hoc* comparisons with Bonferroni correction. However, we limited our comparisons to those

732 chosen *a priori* to be relevant to the interpretation of our study to avoid an overly conservative
733 adjustment of critical p-values as required by Bonferroni correction. To compare the impact of
734 different treatments on IOP and outflow facility, we computed the difference between the
735 treatment groups and their respective injection controls. Subsequently, we conducted two-tailed
736 t-tests with Bonferroni correction. Given the log-transformation of facility data, the subtracted
737 values became ratios upon inverse transformation. To check for consistency between IOP and
738 outflow facility measurements, we calculated residuals as the difference between the expected
739 and experimentally-measured IOPs. A two-tailed t-test was then performed on these residuals
740 with $H_0: \mu = 0$. Pearson correlation test was used measure the relation between TM cellular
741 density and IOP. All analyses were done using MATLAB (v2020, MathWorks, Natick, MA, USA).
742 A significance level of 5% was employed for all tests, unless explicitly stated otherwise.

743 **6. References**


744 1. Y.-C. Tham, X. Li, T. Y. Wong, H. A. Quigley, T. Aung, C.-Y. Cheng, Global prevalence of
745 glaucoma and projections of glaucoma burden through 2040: a systematic review and meta-
746 analysis. *Ophthalmology* **121**, 2081–2090 (2014).

747 2. A. L. Coleman, S. Miglior, Risk factors for glaucoma onset and progression. *Surv. Ophthalmol.*
748 **53**, S3–S10 (2008).

749 3. G. Reardon, S. Kotak, G. F. Schwartz, Objective assessment of compliance and persistence
750 among patients treated for glaucoma and ocular hypertension: a systematic review. *Patient*
751 *Prefer. Adherence* , 441–463 (2011).

752 4. A. Heijl, M. C. Leske, B. Bengtsson, L. Hyman, B. Bengtsson, M. Hussein, E. M. G. T. Group,
753 Reduction of intraocular pressure and glaucoma progression: results from the Early Manifest
754 Glaucoma Trial. *Arch. Ophthalmol.* **120**, 1268–1279 (2002).

755 5. J. Alvarado, C. Murphy, R. Juster, Trabecular Meshwork Cellularity in Primary Open-angle
756 Glaucoma and Nonglaucomatous Normals. *Ophthalmology* **91**, 564–579 (1984).

757 6. R. Manuguerra-Gagné, P. R. Boulos, A. Ammar, F. A. Leblond, G. Krosl, V. Pichette, M. R.
758 Lesk, D.-C. Roy, Transplantation of mesenchymal stem cells promotes tissue regeneration in a
759 glaucoma model through laser-induced paracrine factor secretion and progenitor cell recruitment.
760 *Stem Cells* **31**, 1136–1148 (2013).

761 7. C. Roubeix, D. Godefroy, C. Mias, A. Sapienza, L. Riancho, J. Degardin, V. Fradot, I. Ivkovic,
762 S. Picaud, F. Sennlaub, Intraocular pressure reduction and neuroprotection conferred by bone
763 marrow-derived mesenchymal stem cells in an animal model of glaucoma. *Stem Cell Res. Ther.*
764 **6**, 1–13 (2015).

765 8. D. W. Abu-Hassan, X. Li, E. I. Ryan, T. S. Acott, M. J. Kelley, Induced Pluripotent Stem Cells
766 Restore Function in a Human Cell Loss Model of Open-Angle Glaucoma. *Stem Cells* **33**, 751–
767 761 (2015).

768 9. W. Zhu, O. W. Gramlich, L. Laboissonniere, A. Jain, V. C. Sheffield, J. M. Trimarchi, B. A.
769 Tucker, M. H. Kuehn, Transplantation of iPSC-derived TM cells rescues glaucoma phenotypes in
770 vivo. *Proc. Natl. Acad. Sci.* **113**, E3492–E3500 (2016).

771 10. W. Zhu, A. Jain, O. W. Gramlich, B. A. Tucker, V. C. Sheffield, M. H. Kuehn, Restoration of
772 aqueous humor outflow following transplantation of iPSC-derived trabecular meshwork cells in a
773 transgenic mouse model of glaucoma. *Invest. Ophthalmol. Vis. Sci.* **58**, 2054–2062 (2017).

774 11. H. Yun, Y. Wang, Y. Zhou, A. Kumar, K. Wang, M. Sun, D. B. Stolz, X. Xia, C. R. Ethier, Y.
775 Du, Human stem cells home to and repair laser-damaged trabecular meshwork in a mouse model.
776 *Commun. Biol.* **1**, 216 (2018).

777 12. W. Zhu, C. R. Godwin, L. Cheng, T. E. Scheetz, M. H. Kuehn, Transplantation of iPSC-TM
778 stimulates division of trabecular meshwork cells in human eyes. *Sci. Rep.* **10**, 2905 (2020).

779 13. Y. Zhou, X. Xia, E. Yang, Y. Wang, K. G. Marra, C. R. Ethier, J. S. Schuman, Y. Du, Adipose-
780 derived stem cells integrate into trabecular meshwork with glaucoma treatment potential. *FASEB*
781 *J. Off. Publ. Fed. Am. Soc. Exp. Biol.* **34**, 7160 (2020).

782 14. S. Xiong, A. Kumar, S. Tian, E. E. Taher, E. Yang, P. R. Kinchington, X. Xia, Y. Du, M. Pera,
783 M. E. Bronner, Eds. Stem cell transplantation rescued a primary open-angle glaucoma mouse
784 model. *eLife* **10**, e63677 (2021).

785 15. M. R. Bahrani Fard, J. Chan, G. Sanchez Rodriguez, M. Yonk, S. R. Kuturu, A. T. Read, S.
786 Y. Emelianov, M. H. Kuehn, C. R. Ethier, Improved magnetic delivery of cells to the trabecular
787 meshwork in mice. *Exp. Eye Res.* **234**, 109602 (2023).

788 16. X. Wang, Q. Cao, S. Wu, M. R. Bahrani Fard, N. Wang, J. Cao, W. Zhu, Magnetic Nano-
789 Platform Enhanced iPSC-Derived Trabecular Meshwork Delivery and Tracking Efficiency. *Int. J.*
790 *Nanomedicine* **17**, 1285–1307 (2022).

791 17. B. M. Braunger, B. Ademoglu, S. E. Koschade, R. Fuchshofer, T. G. B'Ann, J. A. Kiland, E.
792 A. Hennes-Beann, K. G. Brunner, P. L. Kaufman, E. R. Tamm, Identification of adult stem cells in
793 Schwalbe's line region of the primate eye. *Invest. Ophthalmol. Vis. Sci.* **55**, 7499–7507 (2014).

794 18. M. M. Lalu, L. McIntyre, C. Pugliese, D. Fergusson, B. W. Winston, J. C. Marshall, J. Granton,
795 D. J. Stewart, Safety of Cell Therapy with Mesenchymal Stromal Cells (SafeCell): A Systematic
796 Review and Meta-Analysis of Clinical Trials. *PLOS ONE* **7**, e47559 (2012).

797 19. D. E. Rodríguez-Fuentes, L. E. Fernández-Garza, J. A. Samia-Meza, S. A. Barrera-Barrera,
798 A. I. Caplan, H. A. Barrera-Saldaña, Mesenchymal Stem Cells Current Clinical Applications: A
799 Systematic Review. *Arch. Med. Res.* **52**, 93–101 (2021).

800 20. Q. J. Ding, W. Zhu, A. C. Cook, K. R. Anfinson, B. A. Tucker, M. H. Kuehn, Induction of
801 trabecular meshwork cells from induced pluripotent stem cells. *Invest. Ophthalmol. Vis. Sci.* **55**,
802 7065–7072 (2014).

803 21. H. Friedman, N. Ator, N. Haigwood, W. Newsome, J. S. Allan, T. G. Golos, J. H. Kordower,
804 R. E. Shade, M. E. Goldberg, M. R. Bailey, P. Bianchi, The Critical Role of Nonhuman Primates
805 in Medical Research. *Pathog. Immun.* **2**, 352–365 (2017).

22. T. Acott, J. R. Samples, J. M. Bradley, D. R. Bacon, S. S. Bylsma, E. M. Van Buskirk, Trabecular Repopulation by Anterior Trabecular Meshwork Cells After Laser Trabeculoplasty: Reply. *Am. J. Ophthalmol.* **108**, 210 (1989).

23. R. M. Sappington, B. J. Carlson, S. D. Crish, D. J. Calkins, The Microbead Occlusion Model: A Paradigm for Induced Ocular Hypertension in Rats and Mice. *Invest. Ophthalmol. Vis. Sci.* **51**, 207–216 (2010).

24. J. C. Morrison, C. G. Moore, L. M. Deppmeier, B. G. Gold, C. K. Meshul, E. C. Johnson, A rat model of chronic pressure-induced optic nerve damage. *Exp. Eye Res.* **64**, 85–96 (1997).

25. A. J. Turner, R. Vander Wall, V. Gupta, A. Klistorner, S. L. Graham, DBA/2J mouse model for experimental glaucoma: pitfalls and problems. *Clin. Experiment. Ophthalmol.* **45**, 911–922 (2017).

26. G. S. Zode, M. H. Kuehn, D. Y. Nishimura, C. C. Searby, K. Mohan, S. D. Grozdanic, K. Bugge, M. G. Anderson, A. F. Clark, E. M. Stone, V. C. Sheffield, Reduction of ER stress via a chemical chaperone prevents disease phenotypes in a mouse model of primary open angle glaucoma. *J. Clin. Invest.* **121**, 3542–3553 (2011).

27. R. F. Brubaker, Goldmann's equation and clinical measures of aqueous dynamics. *Exp. Eye Res.* **78**, 633–637 (2004).

28. G. Li, C. Lee, A. T. Read, K. Wang, J. Ha, M. Kuhn, I. Navarro, J. Cui, K. Young, R. Gorijavolu, Anti-fibrotic activity of a rho-kinase inhibitor restores outflow function and intraocular pressure homeostasis. *Elife* **10**, e60831 (2021).

29. D. R. Overby, J. Bertrand, O.-Y. Tektas, A. Boussommier-Calleja, M. Schicht, C. R. Ethier, D. F. Woodward, W. D. Stamer, E. Lütjen-Drecoll, Ultrastructural Changes Associated With Dexamethasone-Induced Ocular Hypertension in Mice. *Invest. Ophthalmol. Vis. Sci.* **55**, 4922–4933 (2014).

30. C. R. Ethier, R. D. Kamm, B. A. Palaszewski, M. C. Johnson, T. M. Richardson, Calculations of flow resistance in the juxtacanalicular meshwork. *Invest. Ophthalmol. Vis. Sci.* **27**, 1741–1750 (1986).

31. F. J. Wippold, A. Perry, Neuropathology for the Neuroradiologist: Rosettes and Pseudorosettes. *AJNR Am. J. Neuroradiol.* **27**, 488–492 (2006).

32. M. J. Moore, J. A. Sebastian, M. C. Kolios, Determination of cell nucleus-to-cytoplasmic ratio using imaging flow cytometry and a combined ultrasound and photoacoustic technique: a comparison study. *J. Biomed. Opt.* **24**, 106502 (2019).

33. S. J. Coulon, J. S. Schuman, Y. Du, M. R. B. Fard, C. R. Ethier, W. D. Stamer, A novel glaucoma approach: Stem cell regeneration of the trabecular meshwork. *Prog. Retin. Eye Res.* **90**, 101063 (2022).

34. G. Li, C. Lee, V. Agrahari, K. Wang, I. Navarro, J. M. Sherwood, K. Crews, S. Farsiu, P. Gonzalez, C.-W. Lin, A. K. Mitra, C. R. Ethier, W. D. Stamer, In vivo measurement of trabecular meshwork stiffness in a corticosteroid-induced ocular hypertensive mouse model. *Proc. Natl. Acad. Sci. U. S. A.* **116**, 1714–1722 (2019).

844 35. Y. Qiu, H. Yang, B. Lei, Effects of three commonly used anesthetics on intraocular pressure
845 in mouse. *Curr. Eye Res.* **39**, 365–369 (2014).

846 36. T. G. Graber, L. Ferguson-Stegall, J.-H. Kim, L. V. Thompson, C57BL/6 Neuromuscular
847 Healthspan Scoring System. *J. Gerontol. A. Biol. Sci. Med. Sci.* **68**, 1326–1336 (2013).

848 37. R. Fuchshofer, U. Welge-Lussen, E. Lütjen-Drecoll, The effect of TGF-β2 on human trabecular
849 meshwork extracellular proteolytic system. *Exp. Eye Res.* **77**, 757–765 (2003).

850 38. R. C. Tripathi, J. Li, W. F. Chan, B. J. Tripathi, Aqueous humor in glaucomatous eyes contains
851 an increased level of TGF-beta 2. *Exp. Eye Res.* **59**, 723–727 (1994).

852 39. E. R. Tamm, R. Fuchshofer, What Increases Outflow Resistance in Primary Open-angle
853 Glaucoma? *Surv. Ophthalmol.* **52**, S101–S104 (2007).

854 40. S. Neri, Genetic Stability of Mesenchymal Stromal Cells for Regenerative Medicine
855 Applications: A Fundamental Biosafety Aspect. *Int. J. Mol. Sci.* **20**, 2406 (2019).

856 41. N. Lamm, U. Ben-David, T. Golan-Lev, Z. Storchová, N. Benvenisty, B. Kerem, Genomic
857 Instability in Human Pluripotent Stem Cells Arises from Replicative Stress and Chromosome
858 Condensation Defects. *Cell Stem Cell* **18**, 253–261 (2016).

859 42. S. Yamanaka, Pluripotent Stem Cell-Based Cell Therapy-Promise and Challenges. *Cell Stem*
860 *Cell* **27**, 523–531 (2020).

861 43. L. Olson, Å. Seiger, Brain tissue transplanted to the anterior chamber of the eye. *Z. Für*
862 *Zellforsch. Mikrosk. Anat.* **135**, 175–194 (1972).

863 44. E. Inagaki, E. Arai, S. Hatou, T. Sayano, H. Taniguchi, K. Negishi, Y. Kanai, Y. Sato, H. Okano,
864 K. Tsubota, S. Shimmura, The Anterior Eye Chamber as a Visible Medium for In Vivo
865 Tumorigenicity Tests. *Stem Cells Transl. Med.* **11**, 841–849 (2022).

866 45. C. W. Boone, L. T. DuPree, Quantitative tumorigenicity assays using the anterior chamber of
867 the mouse eye. *Cancer Res.* **28**, 1734–1737 (1968).

868 46. A. J. Burand Jr, L. Di, L. K. Boland, D. T. Boyt, M. V. Schrodt, D. A. Santillan, J. A. Ankrum,
869 Aggregation of human mesenchymal stromal cells eliminates their ability to suppress human T
870 cells. *Front. Immunol.* **11**, 143 (2020).

871 47. F. Progatzky, M. J. Dallman, C. Lo Celso, From seeing to believing: labelling strategies for in
872 vivo cell-tracking experiments. *Interface Focus* **3**, 20130001 (2013).

873 48. H. Yun, K. L. Lathrop, E. Yang, M. Sun, L. Kagemann, V. Fu, D. B. Stolz, J. S. Schuman, Y.
874 Du, A Laser-Induced Mouse Model with Long-Term Intraocular Pressure Elevation. *PLOS ONE*
875 **9**, e107446 (2014).

876 49. S. W. John, J. R. Hagaman, T. E. MacTaggart, L. Peng, O. Smithes, Intraocular pressure in
877 inbred mouse strains. *Invest. Ophthalmol. Vis. Sci.* **38**, 249–253 (1997).

878 50. V. K. Raghunathan, J. Benoit, R. Kasetti, G. Zode, M. Salemi, B. S. Phinney, K. E. Keller, J.
879 A. Staverosky, C. J. Murphy, T. Acott, J. Vranka, Glaucomatous cell derived matrices differentially

880 modulate non-glaucomatous trabecular meshwork cellular behavior. *Acta Biomater.* **71**, 444–459
881 (2018).

882 51. C. M. McDowell, K. Kizhatil, M. H. Elliott, D. R. Overby, J. van Batenburg-Sherwood, J. C.
883 Millar, M. H. Kuehn, G. Zode, T. S. Acott, M. G. Anderson, Consensus recommendation for mouse
884 models of ocular hypertension to study aqueous humor outflow and its mechanisms. *Invest.*
885 *Ophthalmol. Vis. Sci.* **63**, 12–12 (2022).

886 52. S. Tsuchiya, T. Higashide, S. Hatake, K. Sugiyama, Effect of inhalation anesthesia with
887 isoflurane on circadian rhythm of murine intraocular pressure. *Exp. Eye Res.* **203**, 108420 (2021).

888 53. J. M. Sherwood, E. Reina-Torres, J. A. Bertrand, B. Rowe, D. R. Overby, Measurement of
889 outflow facility using iPerfusion. *PloS One* **11**, e0150694 (2016).

890 54. G. Li, C. Lee, V. Agrahari, K. Wang, I. Navarro, J. M. Sherwood, K. Crews, S. Farsiu, P.
891 Gonzalez, C.-W. Lin, A. K. Mitra, C. R. Ethier, W. D. Stamer, In vivo measurement of trabecular
892 meshwork stiffness in a corticosteroid-induced ocular hypertensive mouse model. *Proc. Natl.*
893 *Acad. Sci. U. S. A.* **116**, 1714–1722 (2019).

894 55. C. A. Schneider, W. S. Rasband, K. W. Eliceiri, NIH Image to ImageJ: 25 years of image
895 analysis. *Nat. Methods* **9**, 671–675 (2012).

896 56. N. Sadeghiani, L. S. Barbosa, L. P. Silva, R. B. Azevedo, P. C. Morais, Z. G. M. Lacava,
897 Genotoxicity and inflammatory investigation in mice treated with magnetite nanoparticles surface
898 coated with polyaspartic acid. *J. Magn. Magn. Mater.* **289**, 466–468 (2005).

899 57. A. Stroh, C. Zimmer, C. Gutzeit, M. Jakstadt, F. Marschinke, T. Jung, H. Pilgrimm, T. Grune,
900 Iron oxide particles for molecular magnetic resonance imaging cause transient oxidative stress in
901 rat macrophages. *Free Radic. Biol. Med.* **36**, 976–984 (2004).

902 58. N. Singh, G. J. S. Jenkins, R. Asadi, S. H. Doak, Potential toxicity of superparamagnetic iron
903 oxide nanoparticles (SPION). *Nano Rev.* **1**, 5358 (2010).

904

905 **7. Acknowledgements**

906 *Funding*

907 National Institutes of Health grant R01 EY030071 (CRE, SYE, MHK)

908 The Georgia Research Alliance (CRE).

909 *Author Contributions*

910 Conceptualization: CRE, MRBF, MHK, SYE

911 Methodology: MRBF, CRE, MHK, LC, JC, ATR, GL, AJ, HEG, WDS, BNS, SMS

Investigation: MRBF, CRE

Visualization: MRBF, CRE

Funding acquisition: CRE, MHK, SYE

Project administration: CRE, MRBF

Supervision: CRE

Writing – original draft: MRBF, CRE

Writing – review & editing: MRBF, JC, ATR, GL, LC, BNS, SMS, AJ, HEG, SYE, WDS, MHK, CRE

# SUPPLEMENTARY MATERIALS

## S.1 Supplementary figures

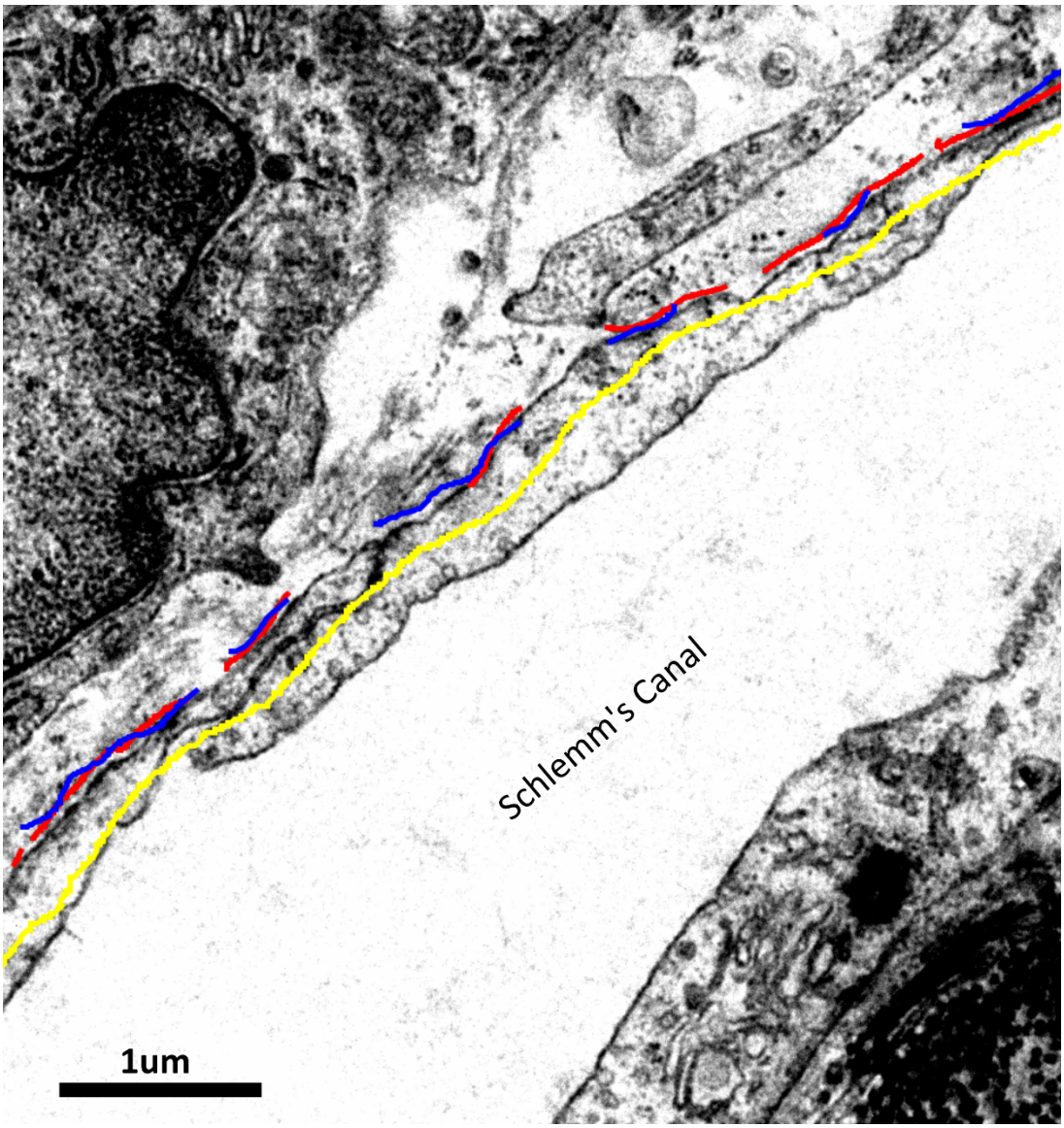


Supplementary Figure 1. Quantification procedure for the amount of basement membrane materials (BMM) underlying to the inner wall of Schlemm's canal. The red and blue line segments mark the basement membrane materials adjacent to the inner wall of Schlemm's canal for each annotator. The summed length of these segments was then normalized by the overall length of

the inner wall (yellow) for quantifications. The yellow line is slightly shifted from the blue and red segments for easier visualization.

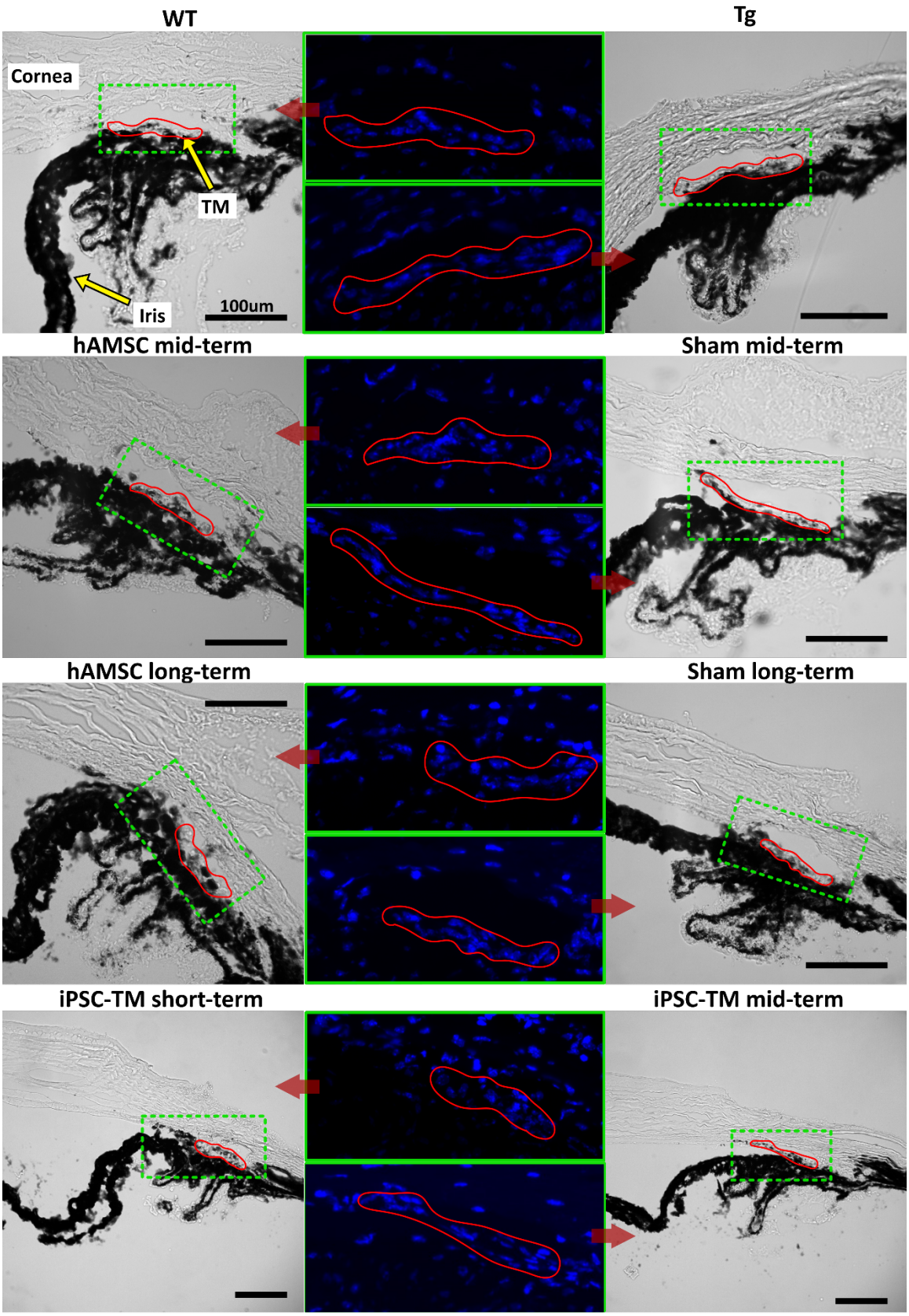
WT
Tg
Cornea
TM
Iris
100um
hAMSC mid-term
Sham mid-term
hAMSC long-term
Sham long-term
iPSC-TM short-term
iPSC-TM mid-term

929

Supplementary Figure 2. Complementary micrographs to Figure 4 used for TM cellularity quantifications. Overview micrographs are shown in the left and right columns (see labels above images), with zoomed regions in the central column as indicated by the red arrows. Regions of interest (ROI), encompassing the parts of TM used for nuclei counting (demarcated in red) are outlined by green dashed boxes and the DAPI-stained nuclei (blue) are shown in a zoomed-in fluorescent micrograph of the ROI (green solid box). In overview images in which the ROI is tilted, the corresponding fluorescent micrograph has been rotated counterclockwise so that it is horizontal, thus enabling a more compact presentation.

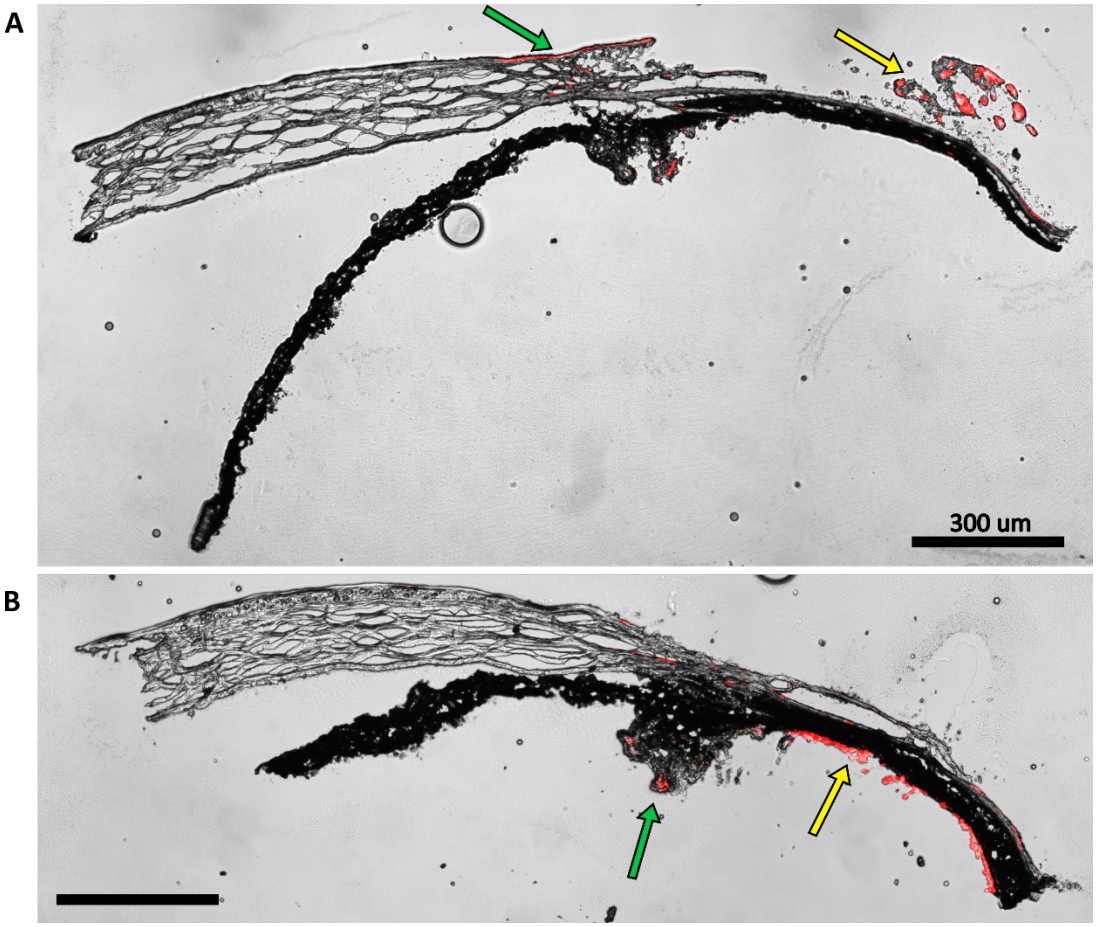


Supplementary Figure 3. Autofluorescence from various ocular tissues at the same fluorescence settings as used in Figure 6. The autofluorescence profile is dependent on the quality of dissection. In A, a signal is evident in insufficiently removed orbital tissue (yellow arrow) and at the limbus (green arrow). In B, autofluorescence is localized within the remnants of the retina (yellow arrow) and ciliary body (green arrow).

Supplementary Table 1. IOP measurements for select groups, shown as means and [95% confidence intervals] similar to Table 1. Tg Mid: Untreated eyes, either contralateral to sham mid-term or hAMSC Mid-term eyes (n = 23).

| Group | IOP (mmHg) |
|---|---|
| WT | 15.6 [14.8,16.3] |
| Tg | 15.4 [14.7,16.1] |
| Tg Mid | 16.5 [15.9,17.1] |
| Sham Mid | 16.9 [15.5,18.2] |

Supplementary Table 2. Result of multiple comparison for the groups listed in Supplementary Table 1. None of the comparisons reached statistical significance.

| | Compared groups | | |
|---|---|---|---|
| | Vs. | | p-value* |
| 1 | WT | Tg | 0.3579 |
| 2 | WT | Tg Mid | 0.0680 |
| 3 | WT | Sham Mid | 0.0491 |
| 4 | Tg | Tg Mid | 0.0278 |
| 5 | Tg | Sham Mid | 0.0311 |
| 6 | Tg Mid | Sham Mid | 0.5148 |

* Post-hoc comparisons were performed after ANOVA. Bonferroni correction was used to adjust the critical p-value from 0.05 to 0.008 (based on the 6 reported comparisons).

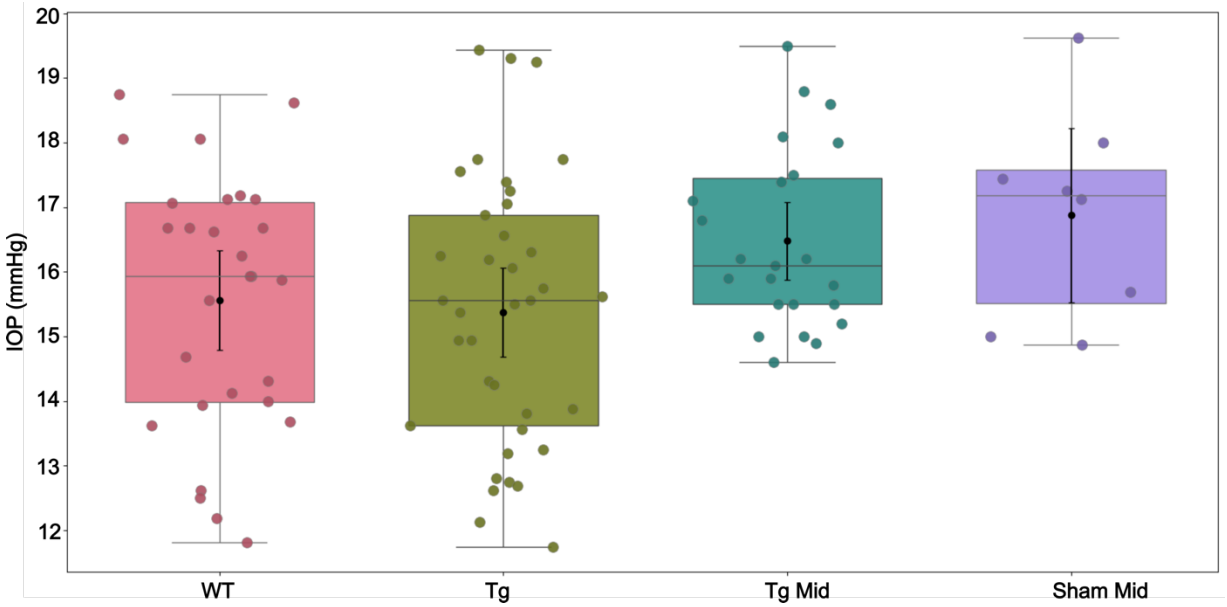


Supplementary Figure 4. IOP measurements corresponding to Supplementary Table 1. In each experimental cohort, the box plot shows interquartile range, and the center horizontal line denotes median. Black dots and its whiskers show the mean and 95% confidence interval on the mean,

955 respectively. Dots represent individual eyes. See Supplementary Table 2 for complete statistical
956 analysis.

957 **S.2 SPION visualization post-transplantation**

958 For reasons described below, it was useful to know where SPIONs had accumulated within the
959 eye. We therefore carried out histological analyses of tissue sections to visualize SPIONs, Using
960 a Prussian blue staining process.

961 *S.2.1 Prussian blue staining of SPIONs*

962 A Prussian blue solution was freshly prepared by mixing a 1:1 ratio of a 20% aqueous solution of
963 hydrochloric acid and a 10% aqueous solution of potassium ferrocyanide (K4Fe(CN)6·3H2O,
964 Sigma-Aldrich). Cryosections from the eyes which were sampled for cell retention studies were
965 rehydrated for 30 minutes. Subsequently, the sections were covered with the 10% potassium
966 ferrocyanide solution for 5 minutes, followed by a 15-minute treatment with the Prussian blue
967 solution. After treatment, the sections were rinsed three times in distilled water, dehydrated
968 through increasing concentrations of ethanol, cleared in xylene, and then mounted for imaging.

969 *S.2.2 SPIONs co-located with exogenous cells post-transplantation*

970 A major concern regarding the use of SPIONs for cell encapsulation is dose-dependent toxicity
971 which could damage both the transplanted cells and native tissues *(56, 57)*. We therefore
972 visualized the SPIONs using Prussian blue staining anterior segment sagittal sections
973 (Supplementary Figure 5). Unfortunately, this dark blue stain proved barely discernable from
974 pigment. Detectible labeling could mostly be found at comparable locations within the AC as in
975 hAMSC-injected eyes (Figure 6B), where both the cells and SPIONs accumulated in the vicinity
976 of TM, and in iPSC-TM-injected eyes (Figure 6B), with the cells and SPIONs found within the TM.
977 Prussian blue did not stain materials in the saline-injected control eyes.

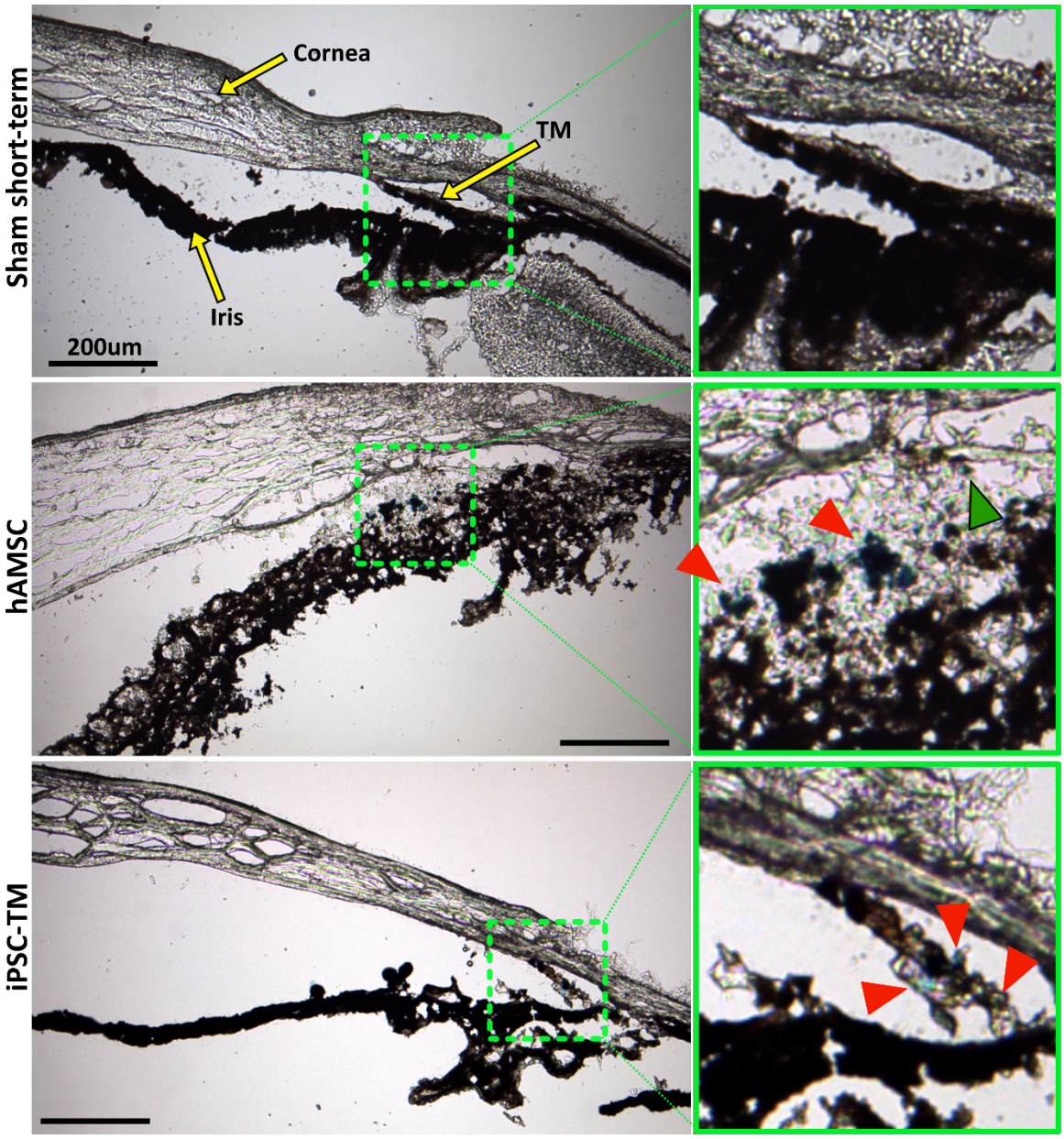


Supplementary Figure 5. Prussian blue staining to locate SPIONs within the anterior segment after cell transplantation. The left column shows overview images of the anterior segment, while green boxes in the right column show a zoomed view of the region with strongest Prussian blue staining, corresponding to the green dashed boxes in the left column. Top row: No Prussian blue staining could be found in the saline injection control. Middle row: Prussian blue stain is challenging to distinguish from melanin, but accumulation of blue label (red arrowheads) can be seen to coincide with the locations of exogenous cells visualized in Figure 6. In particular, injected hAMSCs primarily accumulated close to the TM, corresponding to the location of Prussian blue stain. A small region of Prussian blue staining can be observed in the TM (green arrowhead). Bottom row: Similarly, in eyes receiving iPSC-TMs, most of the Prussian blue staining was found within the TM, corresponding to the location of injected cells (Figure 6). Unfortunately, the fluorescent signal in Figure 6 was significantly attenuated after Prussian blue staining and could

991 not be overlaid on these images to assist with interpretation. Iris degradation, notable in the middle
992 row, is an undesirable artifact of the cryosectioning or staining process (Figure 6).

993 *S.2.3 SPIONs did not accumulate within the native tissues of the AC*

994 Iron oxide-induced toxicity, both as cytotoxicity and genotoxicity, is a major concern when using
995 SPIONs in cell encapsulation and transplantation. *In vitro* studies have reported that SPION
996 labeling is generally safe at concentrations below 100 µg/ml *(58)*. Since we used a four-fold lower
997 concentration for cell labeling in this study, the encapsulated cells were likely unaffected.

998 Once inside the AC, the SPIONs may be released from the injected cells. The TM, as the
999 phagocytic and filtering component of the main AH outflow pathway, is a likely destination. Our
1000 Prussian blue staining to visualize SPIONs in the AC after delivery was masked by pigmentation
1001 and was hard to visualize (Supplementary Figure 5). The SPIONs that we could detect were
1002 mostly co-located with the transplanted cells and were likely not released at a significant rate
1003 within the AC. In the case of iPSC-TM cells, which showed good integration with the TM,
1004 detectable SPIONs were also primarily found within the TM. Whether these SPIONs had been
1005 released from the injected cells or were still encapsulated remains unknown. Nevertheless, the
1006 significant increase in TM cellularity discussed above indicates that accumulation of SPIONs
1007 within the TM is unlikely to have any toxic effect on native tissues.

1008

1009 Table 1. Outcome measures, shown as means and [95% confidence intervals].

| Group | IOP (mmHg) | Facility (nl/min/mmHg) | Cellular Density (nuclei/μm) |
|---|---|---|---|
| WT | 15.6 [14.8,16.3] | 4.4 [3.7,5.2] | 0.24 [0.15,0.33] |
| Tg | 15.4 [14.7,16.1] | 3.8 [3.3,4.4] | 0.28 [0.23,0.32] |
| Sham Short | 17.1 [16.0,18.1] | 3.2 [2.3,4.3] | 0.27 [0.20,0.34] |
| MSC Short | 12.8 [11.9,13.8] | 8.4 [6.3,11.2] | 0.58 [0.42,0.73] |
| Sham Mid | 16.9 [15.5,18.2] | 3.0 [2.1,4.3] | 0.24 [0.18,0.31] |
| MSC Mid | 12.4 [11.6,13.2] | 8.4 [7.1,9.9] | 0.40 [0.34,0.47] |
| Sham Long | 16.7 [16.0,17.5] | 3.4 [2.8,4.2] | 0.23 [0.17,0.28] |
| MSC Long | 12.2 [11.0,13.3] | 8.0 [5.9,10.9] | 0.37 [0.31,0.43] |
| iPSC-TM Short | 14.8 [14.0,15.6] | 4.3 [3.0,6.2] | 0.36 [0.27,0.45] |
| iPSC-TM Mid | 15.0 [14.3,15.7] | 4.3 [3.6,5.1] | 0.34 [0.21,0.47] |

1010 Table 2. Result of multiple comparison for various groups and variables, with statistically
1011 significant comparisons highlighted in orange*.

| | Compared groups | | p-values | | |
|---|---|---|---|---|---|
| | Vs. | | IOP | Facility | Cellular |
| 1 | WT | Tg | 0.3579 | 0.1353 | 0.6264 |
| 2 | Tg | Sham Short | 0.0070 | 0.0901 | 0.9214 |

| | | | | | |
|---|---|---|---|---|---|
| 3 | Tg | Sham Mid | 0.0311 | 0.0614 | 0.2879 |
| 4 | Tg | Sham Long | 0.0652 | 0.1865 | 0.2442 |
| 5 | Tg | hAMSC Short | <0.0001 | <0.0001 | <0.0001 |
| 6 | Tg | hAMSC Mid | <0.0001 | <0.0001 | 0.0003 |
| 7 | Tg | hAMSC Mid | <0.0001 | <0.0001 | 0.008 |
| 8 | Tg | iPSC-TM Short | 0.1287 | 0.2044 | 0.0239 |
| 9 | Tg | iPSC-TM Mid | 0.3073 | 0.1296 | 0.0303 |
| 10 | Sham Short | hAMSC Short | <0.0001 | <0.0001 | <0.0001 |
| 11 | Sham Short | iPSC-TM Short | 0.0006 | 0.0692 | 0.0535 |
| 12 | hAMSC Short | hAMSC Mid | 0.2786 | 0.4838 | <0.0001 |
| 13 | hAMSC Short | hAMSC Long | 0.2111 | 0.4045 | <0.0001 |
| 14 | hAMSC Short | iPSC-TM Short | 0.0013 | 0.0019 | <0.0001 |
| 15 | Sham Mid | hAMSC Mid | <0.0001 | <0.0001 | <0.0001 |
| 16 | Sham Mid | iPSC-TM Mid | 0.0047 | 0.0210 | 0.0072 |
| 17 | hAMSC Mid | hAMSC Long | 0.3497 | 0.3719 | 0.5595 |
| 18 | hAMSC Mid | iPSC-TM Mid | <0.0001 | <0.0001 | 0.2751 |
| 19 | Sham Long | hAMSC Long | <0.0001 | <0.0001 | 0.0020 |
| 20 | iPSC-TM Short | iPSC-TM Mid | 0.3597 | 0.4877 | 0.8516 |

* Post-hoc comparisons were performed after ANOVA (for IOP and outflow facility) or linear mixed-effect model (for TM cellularity). Bonferroni correction was used to adjust the critical p-value from 0.05 to 0.0025 (based on the 20 reported comparisons).